Available online at www.sciencedirect.com
SCIENCE DIRECT®
Journal of Solid State Chemistry 179 (2006) 2394–2415
JOURNAL OF SOLID STATE CHEMISTRY
www.elsevier.com/locate/jssc

A crystallographic description of experimentally identified formation reactions of $Cu(In,Ga)Se_2$

F. Hergert[a,*], S. Jost[a], R. Hock[a], M. Purwins[b]

[a]Chair for Crystallography and Structural Physics, University of Erlangen–Nürnberg, Staudtstraße 3, D-91058 Erlangen, Germany
[b]Crystal Growth Laboratory, Department of Materials Science VI, University of Erlangen-Nürnberg, Martensstr. 7, D-91058 Erlangen, Germany

Received 23 December 2005; received in revised form 24 April 2006; accepted 27 April 2006
Available online 12 May 2006

Abstract

This work describes solid-state reactions for the formation of the chalcopyrite compounds $CuInSe_2$, $CuGaSe_2$ and $Cu(In,Ga)Se_2$ on atomic scale. The most important chalcopyrite formation reactions which were identified by the authors by real-time in situ X-ray diffraction in preceding experiments are (A) $CuSe + InSe \rightarrow CuInSe_2$, (B) $Cu_2Se + 2\ InSe + Se \rightarrow 2\ CuInSe_2$ and (C) $Cu_2Se + In_2Se_3 \rightarrow 2\ CuInSe_2$. During the selenistaion of a metallic precursor containing gallium a separate fourth reaction occurs: (D) $Cu_2Se + Ga_2Se_3 \rightarrow 2\ CuGaSe_2$. The quaternary compound is finally formed by interdiffusion of $CuInSe_2$ with $CuGaSe_2$ (E). These five reactions differ in their activation energy and reaction speed. We explain these differences qualitatively by analysing the involved crystal structures for each reaction. It turns out that all reactions involved in the formation of $Cu(In,Ga)Se_2$ are promoted by epitaxial relations, which facilitates the formation of polycrystalline thin films at temperatures much below those necessary for single crystal growth. Recommendations for the growth of larger grains of $Cu(In,Ga)Se_2$ containing fewer defects are given.

Keywords: Chalcogenide; Crystal growth; Epitaxial growth; Semiconducting materials; Solid state synthesis; Ternary compounds; Thin films

1. Introduction

Polycrystalline $Cu(In,Ga)Se_2$ is a promising absorber material for thin film solar cells [1]. One method to produce this material is called rapid thermal processing of stacked elemental layers (SEL) [2]. In a first step copper, indium, gallium and selenium are deposited on a molybdenum-coated soda-lime glass. This SEL precursor is annealed in a selenium atmosphere where the metals react with selenium forming $Cu(In,Ga)Se_2$ via various binary selenides. The knowledge of the solid-state reactions proceeding during the process is desirable to improve the quality of the absorber material. Polycrystalline absorbers consist of grains separated from each other by grain boundaries, which were shown not to act as recombination zones [3]. Nevertheless, SEM images of absorbers leading to high efficiency devices always show large grains ($>1\,\mu m$). Thus, those solid-state reactions creating large grains should be preferred. As experimentally shown [4,5] and thermodynamically verified [6] this result can be achieved by introducing sodium as a dopant in combination with the correct amount of elemental selenium by annealing SEL. Sodium doping is known to influence the electronic properties of the $Cu(In,Ga)Se_2$ absorber thus increasing the efficiency [7] of the solar cell. Additionally, it supplies gaseous selenium during tempering of SEL [6], but hinders the cation diffusion on the other hand. The latter was shown experimentally for the formation of the quaternary compound $CuIn_{0.75}Ga_{0.25}Se_2$ by interdiffusion [5] of the two ternary chalcopyrites (reaction E).

It is further known that the three stage coevaporation (PVD) process [8] leads to the formation of $Cu(In,Ga)Se_2$ platelets with their {110} faces parallel to the substrate surface, if the {001} axis of the compound In_2Se_3 having formed during the first evaporation stage was oriented parallel to the substrate [9].

All these different experimental observations among numerous others can be qualitatively understood by our crystallographic approach.

*Corresponding author. Fax: +49 9131 85 25182.
E-mail address: frank.hergert@krist.uni-erlangen.de (F. Hergert).

0022-4596/$ - see front matter © 2006 Elsevier Inc. All rights reserved.
doi:10.1016/j.jssc.2006.04.033

Table 1
Selected chemical reactions

	Reaction	ΔH (kJ/mol)	Remarks
(A)	$CuSe + InSe \rightarrow CuInSe_2$	−44	Slow
(B)	$\frac{1}{2}Cu_2Se + InSe + \frac{1}{2}Se \rightarrow CuInSe_2$	−55	Fast
(C)	$\frac{1}{2}Cu_2Se + \frac{1}{2}In_2Se_3 \rightarrow CuInSe_2$	−39	Applied in PVD
—	$CuSe + \frac{1}{2}In_2Se_3 - \frac{1}{2}Se \rightarrow CuInSe_2$	−29	Slow
—	$CuSe_2 + \frac{1}{4}In_4Se_3 - \frac{3}{4}Se \rightarrow CuInSe_2$	−70	Not observed; missing epitaxy
(D)	$\frac{1}{2}Cu_2Se + \frac{1}{2}Ga_2Se_3 \rightarrow CuGaSe_2$	−67	Requires >425 °C
—	$CuSe + GaSe \rightarrow CuGaSe_2$	−37	Not observed; no GaSe as educt
(E)	$\frac{3}{4}CuInSe_2 + \frac{1}{4}CuGaSe_2 \rightarrow CuIn_{0.75}Ga_{0.25}Se_2$	—	Interdiffusion

A–E are experimentally verified [5] for tempering SEL.

2. Formation reactions

The compound semiconductor $Cu(In,Ga)Se_2$ has to form via binary selenide compounds which has been thermodynamically proven [6] for the reaction of a copper indium layer with a selenium layer by annealing. Other production methods like PVD or electrodeposition [10] start from binary selenides directly. Thus we have to focus on solid-state reactions involving the binary selenide compounds. We will not describe all intermediate chemical reactions here, but only those reactions directly resulting in the formation of $CuInSe_2$ or $CuGaSe_2$. We describe five experimentally verified reactions paths (called reactions A–E) [5] plus three additional selected reactions not observed. By this we illustrate why certain combinations of crystal structures cannot easily lead to the formation of the chalcopyrite compounds. All reactions listed in Table 1 are exothermic (see [6] for references of the heat of formation values ΔH).

3. Crystallographic data of involved compounds

As we are describing the formation reactions of technically relevant compounds usually being synthesised on glass substrate, it is enough to restrict to compounds being stable between 200 °C (still below the melting point of selenium) and 600 °C, where the substrate will soften too much. We will classify all compounds by the character of the realised bonding types distinguishing between ionic, covalent and van-der-Waals interaction. The strength of the bonds decreases qualitatively in this sequence. We will regard those compounds as ionic in which each cation is coordinated to selenium, referring to the first coordination polyhedron, only. Any compounds with identical atoms directly connected to each other are denoted as compounds containing covalent or van-der-Waals bonds. The distinction of these two bonding types is done by taking the electron configuration of the involved elements into account.

Since we will look for epitaxial relations in Section 4 it is helpful to estimate which facets will be developed by the crystal structures involved in the solid-state reactions. To forecast the favoured lattice planes we apply the law of reticular density discovered by Bravais [11], which was later refined by Niggli [12] and independently therefrom by Donnay and Harker [13]. We will abbreviate this law by using the initials of all four contributors, BNDH. The basic idea of this law is to assume the growing speed of a lattice plane (hkl) to be inversely proportional to its reticular density of atoms. Those lattice planes growing slowest will finally facet the crystal. Although the BNDH law is a quite simple approach to forecast the crystal facets developing close to the thermodynamical equilibrium growth conditions, it is reliable in most cases [14]. A brief review over more sophisticated theories is contained in [15]. We have applied the BNDH law to determine the most favoured facets for each structure by calculating the largest distances $d(hkl)$ of those lattice planes (hkl) referring to non-extinct reflections $h\,k\,l$. We will use this information to recognise those crystal facets $\{hkl\}$ which are formed and thus can principally serve for epitaxial growth in the chemical solid-state reactions described in Section 4. A SEM picture taken after interrupting the annealing of SEL shows that crystal platelets of γ-CuSe have been formed; they are bordered exclusively by facets obtained by the BNDH law (Fig. 1). This perfect agreement between experimental observation

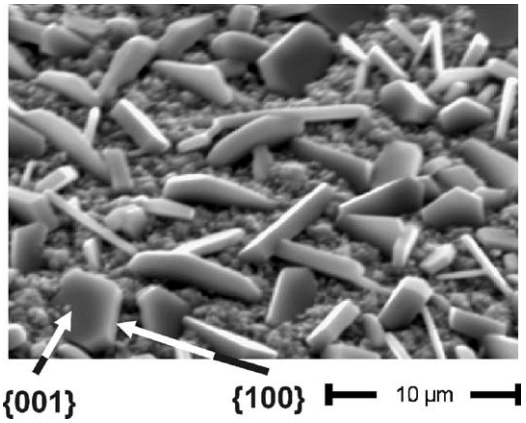

Fig. 1. This SEM picture was taken after interrupting the annealing process with a heating rate of 1 K/s up to 370 °C and quenching with −3.3 K/s, which is fast enough to circumvent the $\gamma \rightarrow \beta \rightarrow \alpha$ phase transition of CuSe. The composition of the film was Cu ÷ In = 11:9 and Se ÷ (Cu + In) = 1.25. The crystal platelets consist of γ-CuSe, showing well-developed {001} and {100} facets. These facets are the two most important ones according to the BNDH law. The platelets are sticking inclined in the SEL precursor layer. Obviously, the material transport, i.e., cations delivered from the metallic sublayer, took place perpendicular to the {001} direction, or, in between the γ-CuSe motif layers (find definition below). This explains, why the {001} facets are best pronounced, as well as why the platelets stick out of the precursor.

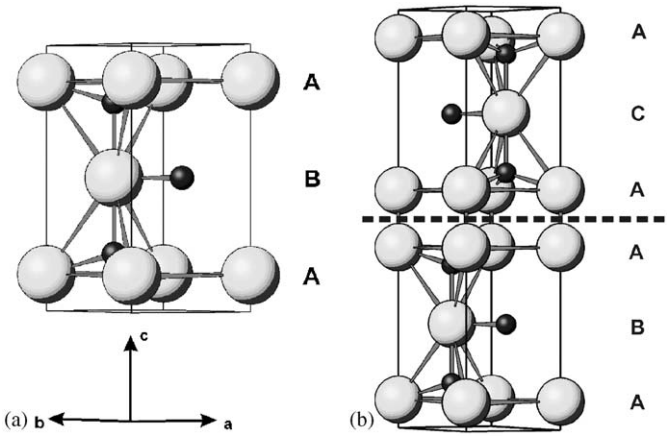

Fig. 2. The structure of γ-CuSe (b) consists of two stacked motifs (a). The stacking sequence of the Se^{2-} anion layers is indicated by capital letters. Cu^{+}: dark, Se^{-}: bright balls.

and prediction confirms once more that the BNDH law holds true, even for crystal growth at steadily increasing temperature.

The Miller indices used for trigonal structures always refer to hexagonal axes. The abbreviations for point symmetry and space groups refer to the international standards [16]. The structure representation was done with the software "PowderCell" [17]. In all figures the radii of the atoms are half the size of the "crystal radii" r for tetrahedral coordination: $r(Cu^{+}) = 74$ pm, $r(In^{3+}) = 76$ pm, $r(Ga^{3+}) = 61$ pm, $r(Na^{+}) = 113$ pm and $r(Se^{2-}) = 184$ pm [18].

One main thought used below to describe epitaxial solid-state reactions in Section 4 is the release of layered crystal structures into their subunits, which we call motifs in the following. These motifs are formulated in a subgroup of the space group of the crystal structure. The idea is as follows: Hexagonal close packed structures are stacked along the ⟨001⟩ axis like ABAB, etc. The atomic arrangement in layers A and B is identical, however the layers are shifted by the translation vector $(\frac{1}{3},\frac{2}{3},\frac{1}{2})$. Hexagonal crystal structures consisting of two identical layers are thus often indicated by adding "2H" to their formula unit. For a cubic close packed crystal structure the stacking sequence is ABCABC, etc. along the ⟨111⟩ direction. The A layer is repeated after a translation of $(\frac{1}{3},\frac{2}{3},\frac{1}{3})$, indicated as B, and a third time after a translation of $(\frac{2}{3},\frac{1}{3},\frac{2}{3})$, called C. The translation vectors refer to the hexagonal setting. The unit cell can be reduced to one third of its volume choosing rhombohedral axes. This is the reason, why this way of stacking is usually abbreviated as "3R". To describe the surface of these layers perpendicular to their stacking direction, it is sufficient to restrain to one layer, being the motif of the whole structure. Using the crystal structure of γ-CuSe as example, we want to illustrate how the motif is derived in this case.

The hexagonal crystal structure of γ-CuSe contains one motif repeating twice along the ⟨001⟩ axis. Thus, we regard this structure as a 2H type (Fig. 2a). To obtain the subcell containing only one motif we have to cut the unit cell of γ-CuSe perpendicular to the ⟨001⟩ axis at $z = \frac{1}{2}$. After this step each half contains one motif (Fig. 2b). Consequently, the lattice parameters c of the substructure will be one half of that for the unit cell of γ-CuSe. Additionally, the values z of all fractional atomic coordinates (x,y,z) have to be doubled. For the description of epitaxial reactions it is enough to restrict our considerations to one motif rather than the complete unit cell of γ-CuSe, if we consider epitaxy on the {001} lattice plane.

For crystal structures existing in several polytypes, like InSe or GaSe, the description of epitaxial relations becomes independent of which polytype is present because they differ from each other just by the way of stacking identical motifs.

We will apply the concept of introducing motifs for all layered crystal structures which contain different bonding types (ionic, covalent, van-der-Waals bonds). The weakest bonding type is always connecting the motifs with each other. For example, InSe and GaSe contain covalent bonds within the motifs, which are themselves interconnected by van-der-Waals interaction. β-In_2Se_3 and γ-CuSe are built from ions, whereas the motifs are interconnected by van-der-Waals and covalent bonds, respectively.

3.1. Ionic compounds

3.1.1. $Cu_{2-x}Se$

Two modifications of this compound exist: the α-phase, stable below 123 °C, and the high-temperature β-phase

Table 2
Ion distribution in Cu_2Se at 170 °C, $a = 584.0$ pm [21]

Atom	Wyckoff site	Point symmetry	Coordination	Occupation (atoms)	Remarks
Se	4*a*	−43*m*	Tetrahedral	4	Sphalerite type sublattice, not ion conductive
Cu	4*c*	−43*m*	Tetrahedral	4	
Cu	4*b*	−43*m*	Octahedral	0.8	Causes ion conductivity, Cu^+ transport via
Cu	16*e*	.3*m*	Trigonal	3.2	4b−16e−16e−4b

melting congruently at 1130 °C [19]. In the β-phase of $Cu_{2-x}Se$ the composition can vary as much as $0 \leqslant x \leqslant 0.3$ [20]. For simplicity we confine our considerations to stoichiometrical β-Cu_2Se with $x = 0$. The high-temperature modification β-Cu_2Se crystallises in the cubic space group $F\,-43m$. Its structure consists of an immobile zincblende-type lattice with the excessive copper cations statistically distributed over three different sites (Table 2). This distribution facilitates the cation conductivity of β-Cu_2Se, achieved by mobile Cu^+ cations on the copper sites (4*b*) and (16*e*) [21]. In addition, the electrons are mobile, too, why β-Cu_2Se is an ambipolar ion conductor [22]. The activation energy for the ion conductivity along the ⟨111⟩ direction is extremely low (0.10 eV [23], 0.16 eV [24] both experimental; 0.12 eV [25], calculated). The network of vacant crystallographic sites offers the possibility of efficient Cu^+ transport. Equilibrium shape crystal growth experiments [22] prove that the growing rate, or the cation conductivity, respectively, is minimal along the ⟨111⟩ direction, whereas the maximal growing rate was found along ⟨110⟩. This means that the cation conductivity is maximal perpendicular to the {110} planes, where the structure possesses its largest channel like voids. All ions in the {111} plane are arranged in hexagons (Fig. 3).

The BNDH law lets us expect the {111}, {100} and {110} facets to be preferred. However, due to the cation conductivity there is no homogeneous material transport for growth. Instead, the only facets developing are the {111} planes, as experimentally shown [22].

3.1.2. Ga_2Se_3

This compound is known to crystallise in two modifications. Above 730 °C [19] the high temperature β-phase crystallises as sphalerite type (space group $F{-}43m$; $a = 542.9$ pm [26]). All atoms have the point symmetry $-43m$ with Se^{2-} anions on the (4*a*) and $2\frac{2}{3}$ Ga^{3+} cations statistically occupying the (4*c*) site partially. The mobile cations result in cation conductivity, as in β-Cu_2Se. The sphalerite-type sublattices of both phases are isostructural to each other.

As a consequence of the cation conductivity of the β-phase the BNDH law cannot be applied here, as in the case of β-Cu_2Se. Similarly to β-Cu_2Se we suppose the {111} facets most likely to occur.

Below 730 °C the Ga^{3+} cations are entirely ordered reducing the point symmetry to 1. The α-phase can be regarded as a monoclinic superstructure (space group *Cc*; $a = c = 666$ pm, $b = 1165$ pm and $\beta = 108.12°$ [27]) of the basic distorted sphalerite type of the β-Ga_2Se_3 structure. The Se^{2-} anions are arranged in slightly distorted corrugated hexagons on the {100}, {010} (Fig. 4a) and {001} planes. They are stacked in the sequence AB along the ⟨010⟩ direction (Fig. 4b).

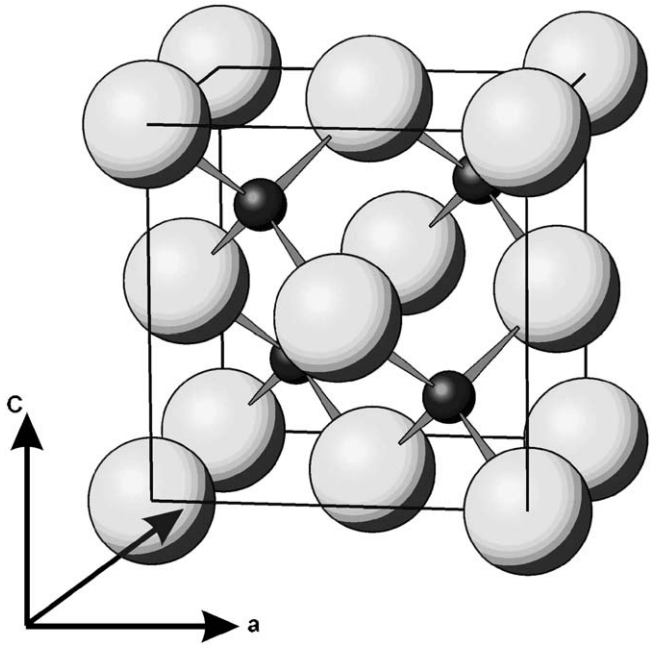

Fig. 3. The zincblende sublattice of β-Cu_2Se and β-Ga_2Se_3. The cations and Se^{2-} anions are each stacked like ABC along the ⟨111⟩ direction. Cu^+: dark, Se^{2-}: bright balls.

We can expect the following facets to develop: {010}, {110}, {−110}, {021} and {111}.

3.1.3. $CuInSe_2$ and $CuGaSe_2$

The isostructural α-phases of both compounds crystallise in the space group $I{-}42d$ (Table 3) in the chalcopyrite structure (Fig. 5a) like $CuFeS_2$ [28]. Neglecting the tetragonal distortion and not distinguishing between the cations, the structures of α-$CuInSe_2$ and α-$CuGaSe_2$ are equal to the immobile zincblende sublattice of β-Cu_2Se with almost equal lattice parameters. The cubic β-modification of the two chalcopyrites can be achieved through a structural phase transition in $CuInSe_2$ at 812 °C [29] and in $CuGaSe_2$ at 1054 °C [30].

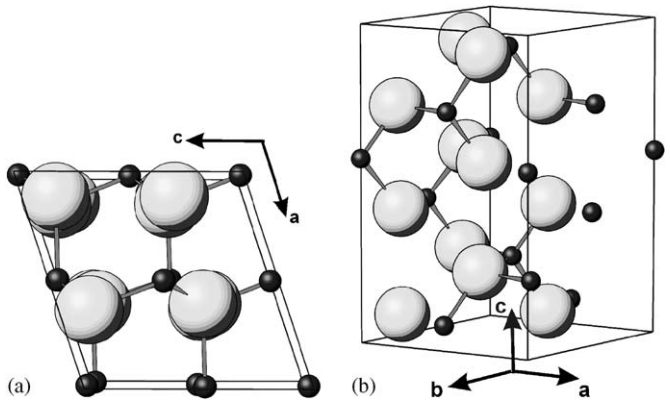

Fig. 4. The monoclinic crystal structure of α-Ga_2Se_3 viewed along its unique axis [010] (a) and as overview (b). The Ga^{3+} cations are arranged in slightly corrugated distorted hexagons. A similar cation alignment is found in the {100} and {001} lattice planes, too. Ga^{3+}: dark, Se^{2-}: bright balls.

Table 3
Crystallographic data of α-$CuInSe_2$ and α-$CuGaSe_2$

Atom	Wyckoff site	x	Point symmetry	Coordination
Cu	4*a*	0	−4..	Tetrahedral, slightly distorted
In/Ga	4*b*	0	−4..	Tetrahedral, slightly distorted
Se	8*d*	0.2271[a]	.2.	Tetrahedral, slightly distorted
		0.259[b]		

[a]For α-$CuInSe_2$ ($a = 578.149$ pm, $c = 1161.879$ pm [31]).
[b]For α-$CuGaSe_2$ ($a = 561.4$ pm, $c = 1102.2$ pm [32]).

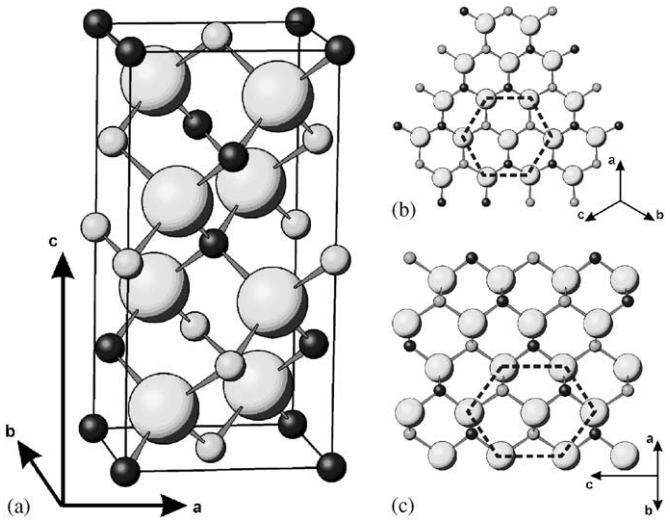

Fig. 5. (a) The crystal structure of the chalcopyrites α-$CuInSe_2$ and α-$CuGaSe_2$. (b) View on the {112} lattice plane (c) Corrugated centred distorted Se^{2-} hexagons are assembled by taking two adjacent layers of the {110}/{102} planes Cu^+: dark, In^{3+} or Ga^{3+}: bright, small balls, Se^{2-}: large bright balls.

It is well probable that the formation reactions described in Section 4 do not directly yield to the tetragonal α-phases, in which the cations are ordered on a long range. As a consequence of the cation exchange the cubic β-phase might form intermediately until the cations have arranged themselves according to the chalcopyrite ordering. We expect such behaviour especially at the interface where the reactions occur. However, an experimental proof is missing, so far.

As $c \approx 2a$ in the α-phase of both chalcopyrites we consider the lattice planes {h k 2l}, {h 1 2k} and {k 1 2h} as symmetrically equivalent, which were exactly fulfilled for $c = 2a$ and $x(\mathrm{Se}) = \frac{1}{4}$. Consequently, the threefold ⟨111⟩ direction of the cubic β-modification corresponds to the ⟨112⟩ direction in the tetragonal α-phase. The Se^{2-} anions are lying in the {112} planes, arranged in centred, slightly distorted hexagons (Fig. 5b). Thus, we can expect the formation of {112} lattice planes of α-$CuInSe_2$ or α-$CuGaSe_2$, if the chalcopyrite compounds are formed by a solid-state reaction from binary compounds containing plane selenium hexagons on their epitaxial facets, as well. This situation occurs for reactions A, B, Cβ and D (Table 8) are discussed later.

In the {110}/{102} planes the Se^{2-} anion sublattice has only twofold symmetry. However, when considering two adjacent lattice planes the Se^{2-} anions of both layers complement to corrugated centred distorted hexagons (Fig. 5c). In the formation reaction Cγ the reactant γ-In_2Se_3 contains corrugated centred distorted hexagons in its {100} lattice plane, like the chalcopyrite structures in their {110}/{102} planes. This is the reason, why in reaction Cγ the {110}/{102} lattice planes are formed, rather than the {112} planes.

Following the BNDH law, the most probable facets in both chalcopyrite structures are the {101}, {112}, {103}, {001} and {100} planes. We like to emphasise that the {110}/{102} planes occur not until the tenth place in the list of possible facets. The observation of the latter, "exotic" facets (see Section 4.3.2) can be understood as a result of epitaxial growth.

The crystal radii r [18] for Cu^+, In^{3+} and Ga^{3+} are small in comparison to that of Se^{2-}. The similarity of the first three cation radii should ease their interdiffusion to form the quaternary mixed crystal compound. $CuIn_{1-x}Ga_xSe_2$ existing for the complete solid solution $0 \leqslant x \leqslant 1$ [33].

3.1.4. γ-In_2Se_3

In_2Se_3 exists in four modifications depending on composition and temperature. We will concentrate on the β- and the γ-phase, which co-exist between 200 and 745 °C [34]. The latter phase is stoichiometrical whereas β-In_2Se_3 is slightly selenium deficient [34] described in Section 3.2.3.

In the crystal structure of γ-In_2Se_3 (space group $P6_1$ or $P6_5$; $a = 712.86$ pm, $c = 1938.1$ pm [35]) all atoms occupy general positions with point symmetry 1. This arrangement

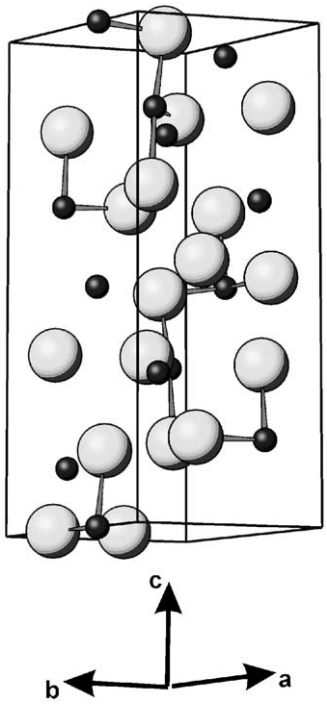

Fig. 6. The γ-In_2Se_3 structure. In^{3+}: dark, Se^{2-}: bright balls.

results in a dense interconnected network of atoms in which atomic diffusion is inhibited (Fig. 6).

The {001} faces are built up from centred hexagons of In^{3+} with a distance of 713 pm. Since the ⟨001⟩ axis is a screw axis, the crystal structure is polar and thus the two {001} faces are allowed to differ from each other. This concerns the anion arrangement: The (001) face contains Se^{2-} anions arranged in plane centred hexagons with 713 pm distance to each other (Fig. 15c). The composition of this face is In:Se = 2:1. Each hexagon contains two Se^{2-} anions. The (00−1) plane has an atomic ratio of In:Se = 1:2 and the Se^{2-} anions are ordered in slightly corrugated distorted non-centred hexagons with an average distance of 413 pm (Fig. 15b). The distance of the Se^{2-} anions projected into the (00−1) plane amounts to 412 pm, calculated from the lattice parameter as $a/\sqrt{3}$. Such a hexagon contains four Se^{2-} anions.

In the {100} planes we find the In^{3+} cations arranged in straight chains running parallel to the unit cell axes a and b with an In–In distance of 713 pm. An easy motif like a hexagonal arrangement cannot be found. The Se^{2-} anions are ordered in distorted centred hexagons. These hexagons are corrugated because four of six Se^{2-} anions are located approximately in the {100} plane whereas the two others are roughly lying on a parallel plane in a distance of 219 pm. The average distance of the Se^{2-} anions calculates to 409 pm.

The ranking of facets obtained by the BNDH law is {100}, {101}, {102}, {103}, {104}, {110}, {111}, {112}, {105} and {001}.

3.2. Compounds containing van-der-Waals bonds

3.2.1. InSe and GaSe

These two diamagnetic compounds contain the dications $[In_2]^{4+}$ and $[Ga_2]^{4+}$ [36]. The exchange of the two outermost s-electrons forming this weak bond between the cations is realised by building layered structures. The selenium anions also arrange in layers, which are only interconnected by weak van-der-Waals interaction. An oxidation to In^{3+} will break the In–In bond perpendicular to the ⟨001⟩ axis due to the release of the two outermost s-electrons. Since the In^{3+} cations will try to achieve tetrahedral coordination with Se^{2-} anions the Se–Se bond perpendicular to the ⟨001⟩ axis has to break up as a consequence, too. The same is valid for the oxidation of the $[Ga_2]^{4+}$ dication.

For both compounds, at least two allotropic structures were observed, differing only in the way of layer stacking along the ⟨001⟩ direction. In all structures each atom has the point symmetry $3m$ and the stacking sequence along the ⟨001⟩ axis is Se–In–In–Se. We therefore restrain our further description on the common subunit Se–In–In–Se, serving as motif, described in the subgroup $P3m1$ (Fig. 7).

The 2H modification of InSe is obtained by stacking two motifs with the translation vector $(\frac{1}{3}, \frac{2}{3}, 1)$, whereas the 3R modification is built up from three motifs, each shifted by $(\frac{2}{3}, \frac{1}{3}, 1)$. For our considerations it is sufficient to restrict the structural description to the motif (Table 4). Moreover, it was experimentally shown that the 2H polytype contains stacking faults along ⟨001⟩ resulting in 2D platelets with a thickness of just one or two motifs [37].

The {001} plane of the structure is built up from regular centred selenium polygons (Fig. 9b).

The BNDH law has to be applied for both InSe polytypes separately. For 2H–InSe we get {001}, {100}, {101}, {102} and {103}, whereas for 3H–InSe the order is {001}, {101}, {002}, {004} and {005}. Thus, we always have to expect {001} facets independent of the polytype which agrees with the observation of thin platelets [37].

Two polytypes [39] of GaSe, 2H ($a = 375.5$ pm, $c = 1594$ pm) and 3R ($a = 375.5$ pm, $c = 2392$ pm), are isostructural to those of InSe. Another 2H polytype (space group: $P{-}6m2$; $a = 374.3$ pm, $c = 1591.9$ pm) has been reported [40]. The GaSe polytypes can be derived from a GaSe motif in analogy to that given for InSe. Therefore, a structural description being independent of stacking faults and resulting polytypism is advantageous. This example underlines the importance to introduce a common structure motif.

Both, GaSe and InSe contain univalent cations. As gallium is located one period above indium in the periodic table of the elements, its univalent oxidation state, Ga^+, is less stable than In^+. This is due to the general trend, that the stability of the highest oxidation state decreases downwards within main groups of the periodic table [41]. Consequently, we follow, that if GaSe and InSe are simultaneously exposed to elemental selenium, GaSe will

selenise at first to Ga_2Se_3, for Ga^{3+} to achieve its most stable oxidation state. In_2Se_3 will not appear, as long as the former reaction is completed. Indeed, the compounds InSe and Ga_2Se_3 have been found to coexist when partially selenising an $CuIn_{0.75}Ga_{0.25}$ alloy [42].

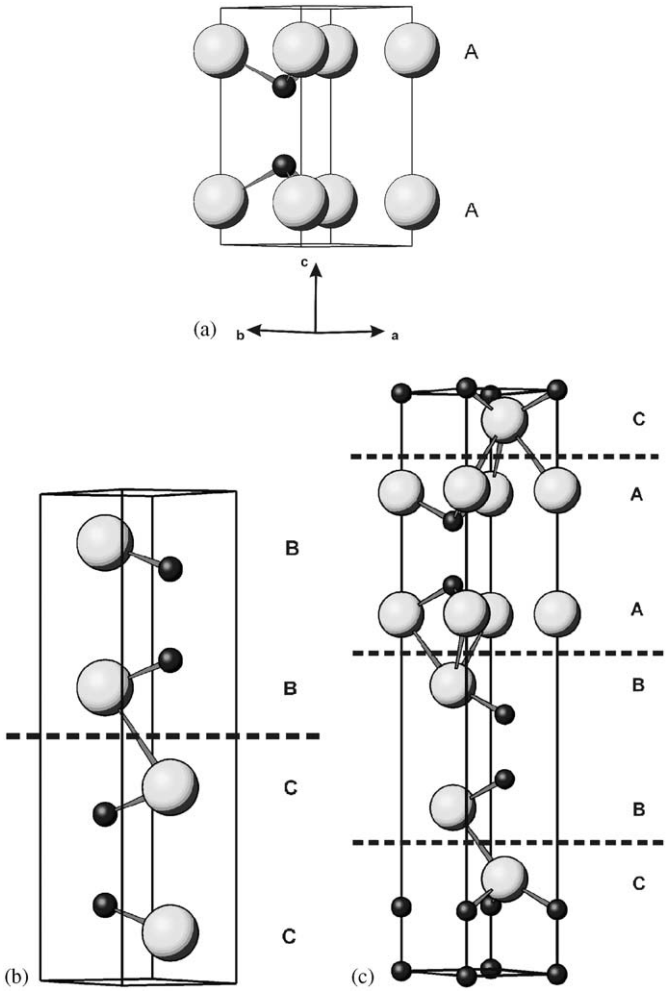

Fig. 7. (a) The structure of the InSe motif, 2H–InSe (b) and 3R-InSe (c) In^{2+}: dark, Se^{2-}: bright balls.

3.2.2. In_6Se_7

This compound can be formally written as $In^+[In_2]^{4+}(In^{3+})_3(Se^{2-})_7$ indicating the presence of In^+ and In^{3+} cations. The crystal structure (space group $P2_1/m$; $a = 943.3$ pm, $b = 406.4$ pm, $c = 1766.3$ pm, $\beta = 100.92^\circ$ [43]) is well interconnected in different directions. Favoured facets are {001}, {100}, {−101}, {101} and {−102}.

3.2.3. β-In_2Se_3

The β-phase is a rhombohedral layered structure with $a = 405$ pm and $c = 2941$ pm [44]. The unit cell contains three formula units stacked in three layers. Each layer corresponds to a motif and can be described in the subgroup $P-3m1$ (Table 5, Fig. 8). The structure can be derived by stacking two motifs with the translation vector $(\frac{1}{3}, \frac{2}{3}, 1)$. The Se–Se bonds connecting these motifs are van-der-Waals type, so that the structure can in principal easily break up along the $\langle 001 \rangle$ axis into its motifs. However, since In^{3+} and Se^{2-} are both present in their most stable oxidation state we cannot expect a redox reaction assisted reaction mechanism destabilising the structure as it is possible for InSe, GaSe or γ-CuSe.

On the {001} plane the structure is built up from centred hexagons of In^{3+} and Se^{2-} (Fig. 13b). Contrary to γ-In_2Se_3, the BNDH law allows the β-phase to develop {001} facets, which coincides with the direction in which van-der-Waals bonding occurs. The ranking list is {001}, {101}, {102}, {104} and {105}.

3.3. Compounds containing covalent bonds without van-der-Waals bonds

3.3.1. γ-CuSe

CuSe is known in three structurally related modifications depending on the temperature [45]. The α-phase, stable at

Table 4
Crystallographic data for 2H–InSe, 3R–InSe and the motif derived from the 2H and 3R polytype

Compound	Space group	Atom	Wyckoff site	z	Point symmetry	a (pm)	c (pm)
InSe (2H, β) [37]	$P\,6_3/m\,m\,c$	In	4*f*	0.157	3 *m.*	405	1693
		Se	4*f*	0.602	3 *m.*		
InSe (3R, γ) [38]	$R\,3\,m$	In	3*a*	0	3 *m*	400.2	2494.6
		In	3*a*	0.11104	3 *m*		
		Se	3*a*	0.61674	3 *m*		
		Se	3*a*	0.82840	3 *m*		
InSe (motif, 2H)	$P\,3\,m\,1$	In	1*b*	0.314	3 *m.*	405	846.5
		In	1*b*	0.684	3 *m.*		
		Se	1*a*	0.204	3 *m.*		
		Se	1*a*	0.796	3 *m.*		
InSe (motif, 3R)	$P\,3\,m\,1$	In	1*b*	0.3334	3 *m.*	400.2	831.53
		In	1*b*	0.6666	3 *m.*		
		Se	1*a*	0.1825	3 *m.*		
		Se	1*a*	0.8175	3 *m.*		

Table 5
Crystallographic data for β-In_2Se_3

Compound	Space group	Atom	Wyckoff site	z	Point symmetry	Coordination
In_2Se_3 (β)	$R-3m$	Se	3*a*	0	$-3m$	Octahedral
		Se	6*c*	0.222	3*m*	Trigonal pyramidal
		In	6*c*	0.401	3*m*	Distorted octahedral
β-In_2Se_3 (motif)	$P-3m1$	Se	1*b*	0.5	$-3m.$	Octahedral
		Se	2*d*	0.166	3*m.*	Trigonal pyramidal
		In	2*d*	0.703	3*m.*	Distorted octahedral

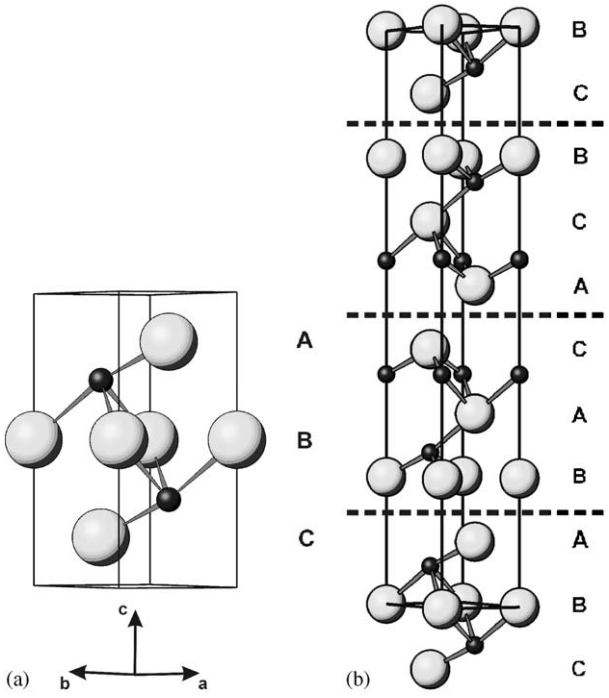

Fig. 8. The β-In_2Se_3 structure (b) and its motif (a). The Se^{2-} anions within each motif are stacked like ABC, which is at the same time the stacking sequence for the motifs. In^{3+}: dark, Se^{2-}: bright balls.

room temperature transforms into the β-phase at 51 °C and the latter into γ-CuSe above 120 °C. The γ-phase finally thermally decomposes at 377 °C into $Cu_{2-x}Se$ and a selenium rich melt [19].

The hexagonal γ-CuSe contains Se–Se layers perpendicular to ⟨001⟩ as InSe and GaSe do. However, since γ-CuSe contains Cu^+ ions [46], the valency of selenium is -1, as known from its polyanion $[Se_2]^{2-}$, which identifies this compound as a polyselenide. As a consequence, the Se–Se layers are interconnected by covalent bonds. There are no metal–metal bonds as in InSe or GaSe, what makes this structure denser packed in comparison: one unit cell of γ-CuSe contains six formula units whereas 2H–InSe or 2H–GaSe contain only four at nearly equal cell dimensions (Table 6). In analogy to the description of InSe, a unit cell for the CuSe-motif was constructed in the subgroup $P-6m2$ containing the atomic sequence Se–Cu–(Cu,Se)–Cu–Se along ⟨001⟩ direction.

One unit cell of γ-CuSe is obtained by stacking of two motives with a rotation of 180° around the ⟨001⟩ axis. The latter is necessary due to the 6_3 screw axis in the space group symbol of the γ-CuSe crystal structure (Fig. 2).

The structure of γ-CuSe contains one Se–Se bond in the coordination polyhedron around Se (4*e*). This distorted tetrahedron is built from one Se (4*e*) and three Cu (4*f*) atoms. If the Se–Se bond is destroyed by reduction of Se^- to Se^{2-}, the structure will break into two halves perpendicular to the ⟨001⟩ direction. In contrast to InSe or GaSe there are no double layers of metal atoms facilitating another separation into {001} layers.

According to the BNDH law the following facets are expected: {001}, {100}, {101}, {102} and {103}. The appearance of the first three during tempering SEL was confirmed by SEM pictures (Fig. 1).

Having in common that γ-CuSe, InSe and GaSe are all layered structures, they will decompose into subunits of different size due to oxidation. The subunits formed are $(CuSe)_3$ in the case of γ-CuSe, whereas the InSe and GaSe structures will at first decompose into their motifs, $(InSe)_2$ and $(GaSe)_2$, and due to oxidation of the cations finally dissolve into units of (InSe) and (GaSe).

3.3.2. In_4Se_3

This compound formally written as $(In^+)[In_3^{5+}](Se^{2-})_3$ contains In^+ and In^{3+} cations (space group *Pnnm*; $a = 1529.6$ pm, $b = 1230.8$ pm, $c = 408.06$ pm [48]). The atoms are connected via a three-dimensional network. Applying the BNDH law gives {110}, {100}, {210}, {010}, {120} as possible facets.

3.3.3. $CuSe_2$

$CuSe_2$ (space group *Pnnm*; $a = 500.5$ pm, $b = 618.2$ pm, $c = 374.0$ pm [49]) is a polyselenide [46] like CuSe, but with the oxidation state $-\frac{1}{2}$ of selenium in the polyanion $[Se_4]^{2-}$. This copper polyselenide forms a dense interconnected network of bonds. A reduction of selenium will break up the covalent bonds and, consecutively, the whole crystal structure.

Expected facets are {110}, {011}, {010}, {101} and {111}.

3.3.4. Selenium

Selenium exists in three crystalline (α, β, γ) and two amorphous modifications [50]. The crystal structure of the

Table 6
Site symmetry in γ-CuSe, $a = 398.0$ pm and $c = 1725.4$ pm at 242 °C [47], the lattice parameters for the motif are a and $c/2$

Compound	Space group	Atom	Wyckoff site	z	Point symmetry	Coordination
CuSe (γ, 2H)	$P6_3/mmc$	Cu	2*d*	$\frac{3}{4}$	$-6m2$	Trigonal planar
		Se	2*c*	$\frac{1}{4}$	$-6m2$	Trigonal bipyramidal
		Cu	4*f*	0.1076	$3m.$	Distorted tetrahedral
		Se	4*e*	0.0687	$3m.$	Distorted tetrahedral
CuSe (motif)	$P-6m2$	Cu	1*f*	0.5	$-6m2$	Trigonal planar
		Se	1*d*	0.5	$-6m2$	Trigonal bipyramidal
		Cu	2*h*	0.7848	$3m.$	Distorted tetrahedral
		Se	2*g*	0.8626	$3m.$	Distorted tetrahedral

grey (metallic) γ-Se is trigonal (space group $P3_121$ or $P3_221$; $a = 436.62$ pm, $c = 495.36$ pm [51]) containing helical selenium chains with a bond angle of 103°. Grey selenium melts at 221 °C [19]. The melt contains selenium chains $[Se_n]$ like in the γ-modification with a temperature-dependent chain length [52]. All bonds are sp^3 hybridised and thus the selenium chains can freely rotate with an ideal bond angle of arccos $(-\frac{1}{3}) \approx 109.5°$.

The selenium chains can be broken up by adding alkali metals in the range of 1 at% to a selenium melt. The valence electrons of the alkali metal will electronically saturate the selenium atoms at the chain endings [53] and subsequently reduce the chain length $m+n$ as follows:

$$[Se_{m+n}]^0 + 2\ Na \rightarrow [Se_{m+n}]^{2-} + 2Na^+,$$

$$[Se_{m+n}]^{2-} + 2\ Na \rightarrow [Se_m]^{2-} + [Se_n]^{2-} + 2\ Na^+.$$

For this reaction the addition of an alkali metal in elemental form is required. We like to emphasise that sodium doping, as applied for the growth of $CuIn(Ga)Se_2$ using different sodium compounds (see [1] and references therein) containing Na^+ cations, will not have this effect. However, we expect the uptake of electrons by the selenium melt as induced by a redox reaction to have the same effect. In this case selenium anions will be released from the selenium chains. This can be derived from the equations above by formal subtraction of Na^+ for $n = 1$:

$$[Se_{m+1}]^{2-} + 2\ e^- \rightarrow [Se_m]^{2-} + Se^{2-}$$

This reaction makes Se^{2-} anions easily available for a solid–liquid interface located anywhere in the highly viscous selenium melt.

4. Crystallographic mechanisms of the formation reactions

In this section, we present reaction mechanisms divided into several subsequent steps for experimentally observed solid-state reactions leading to the chalcopyrite formation. We like to emphasise, that these intermediate reactions will take place simultaneously, especially when regarding more than one unit cell or single motifs. We have tried to identify the most obvious possibility for each solid-state reaction. Easy reaction mechanisms are a good indication for a high probability for the reaction to occur. Reactions A–E are ordered according to the type of bonding in the educts. A comprehensive overview will be given in Section 4.7.

Table 7 comprises atomic distances on selected planes in those structures required for the description of solid-state reactions given below. The deviation of these distances between reacting compounds lies in the range of a few percent. The distances are calculated from the structural data given in Section 3 mostly determined at room temperature if not stated otherwise. To be accurate, the lattice misfit would have to be considered as a function of temperature. However, since these data are not available for most structures, we limit our description of the lattice misfit calculated from the structural data given in Section 3.

If two lattice planes are oriented parallel to each other having (quasi-)identical formed networks, epitaxial growth is likely to occur [54]. The first systematic studies [54] showed that the misfit of the corresponding network spacings tolerated for epitaxy did not exceed ≈15%. Applying this pure geometrical criterion, all compounds listed in Table 7 are suitable for epitaxy in the selected solid-state reactions discussed below. Indeed, epitaxial growth of α-$CuInSe_2$ on β-Cu_2Se has been observed by TEM and a growth model based on the common anion sublattice in both crystal structures has been proposed [55].

The interdiffusion of α-$CuInSe_2$ and α-$CuGaSe_2$ (reaction E) obeys Vegard's law who observed a statistical distribution of the cations in mixed crystal alkali halides [56] and reported that the lattice parameter of a mixed crystal depends linearly on the concentration [57]. Both observations agree with our results from XRD on $Cu(In,Ga)Se_2$ mixed crystals.

4.1. Reaction A: γ-CuSe+InSe→α-$CuInSe_2$

As shown in Section 3.3.1 γ-CuSe is packed ≈ 1.5 times denser along the ⟨001⟩ axis than InSe, whereas the packing density within the {001} planes are equal for both crystal structures. For this reason any plane {*hkl*} with $h \neq 0$ or $k \neq 0$ can be excluded, leaving the {001} plane as the only possibility for epitaxy. As shown above, the {001} facets are likely to occur for γ-CuSe and both InSe

Table 7
Atomic distances of compounds participating in reactions A–E in pm

Phase	2H-InSe	β-In_2Se_3	γ-In_2Se_3		γ-CuSe	α-$CuInSe_2$	
Plane	**{0 0 1}**	**{0 0 1}**	**{1 0 0}**	(0 0−1)	{0 0 1}	**{1 1 2}**	{1 1 0}/{1 0 2}
Cu–Cu	—	—	—	—	398	410	410
In–In	405	405	713[a]	713	—	410	410
Se–Se	405	405	408[b]	413[c]	398	410[d]	410
Phase	2H-GaSe	α-Ga_2Se_3	β-Ga_2Se_3	β-Cu_2Se		α-$CuGaSe_2$	
Plane	**{0 0 1}**	**{0 1 0}**	**{1 1 1}**	**{1 1 1}**	{1 1 0}	**{1 1 2}**	{1 1 0}/{1 0 2}
Cu–Cu	—	—	—	413	413[g]	393	393
Ga–Ga	376	389[e]	384	—	—	393	393
Se–Se	376	391[f]	384	413	413	395[h]	390

In bold: lattice planes forming facets due to BNDH law or anisotrope cation conductivity.
[a]Distance determined along indium chains running parallel to the unit cell axes *a* and *b*.
[b]Average of 36 Se–Se distances (358–455 pm) within the unit cell; distorted centred hexagons.
[c]Average of alternating distances: 389, 400 (2 ×), 421 pm (2 ×) and 431 pm.
[d]Average value of 388, 400 (2 ×), 421 (2 ×) and 431 pm in the distorted hexagons.
[e]Average of 407, 377, 375 (2 ×), 390, 407, 385 and 384 pm; distorted corrugated hexagons.
[f]Average of 375, 408, 381 and 388 pm; distorted corrugated hexagons.
[g]Only the immobile zincblende sublattice taken into account.
[h]Average value of 389, 390 (3 ×) and 397 pm (2 ×) in the distorted hexagons.

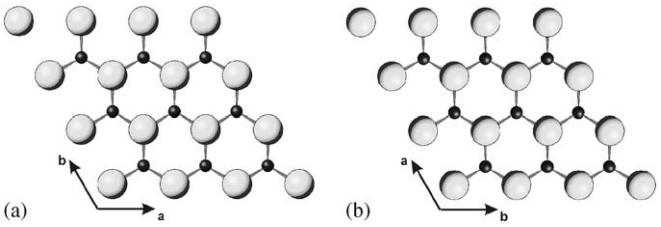

Fig. 9. The {001} plane of γ-CuSe (a) and InSe (b) Cu^+ or In^{3+}: dark, Se^{2-}: bright balls.

polytypes. Since both structures are built up from {001} layers described in $P\,3m1$ it is reasonable to assume epitaxy for both structures on their {001} planes (Fig. 9). The lattice misfit is only 18‰ (6‰) for the 2H (3R) polytype of InSe, respectively. For reaction A we propose the following reaction steps:

1. γ-CuSe and InSe crystals fit epitaxially together on the {001} plane. The absence of dangling bonds on these chemically inactive surfaces is a favourable factor for this kind of epitaxial growth, called van-der-Waals epitaxy [58]. Below we consider a crystal of γ-CuSe having connected to a crystal of InSe at the {001} plane (Fig. 10a).
2. At the interface the following redox reaction is induced transferring copper and selenium ions into their most stable oxidation state:

$$[\mathrm{Se}-\mathrm{Se}]^{2-}\text{in }\gamma_{-\,\mathrm{CuSe}} + [\mathrm{In}-\mathrm{In}]^{4+}{}_{\text{in InSe}} \rightarrow 2\ \mathrm{In}^{3+} + 2\ \mathrm{Se}^{2-}.$$

This equation illustrates that the covalent In–In bonds in InSe and the covalent Se–Se bonds in γ-CuSe break up when the oxidation state is changed. This leads to the formation of CuSe motifs. For InSe we expect not only the In–In but consequently the Se–Se bonds to break up. This will dismount the InSe crystal structure into single layers (half a motif). For simplicity we consider a single motif of γ-CuSe (three layers) being connected to 1.5 motifs of InSe (three layers). This corresponds to three formula units of each compound (Fig. 10a).
3. As a consequence of the redox reaction we can expect the Se–In–In–Se chains along the ⟨001⟩ axis to arrange their ions alternately allowing tetrahedral coordination with the other sort of ions, only. In the CuSe motif, the same argument will shift the atom Cu (1f) along ⟨001⟩ to exchange with the Se (1d) atom. After a translation of the metal–selenium layers by $\pm(\frac{1}{3}, \frac{2}{3}, 0)$, tetrahedral coordination is achieved for all atoms. Fig. 10b shows the realisation for the translation vector being always positive resulting in the stacking sequence ABC of the Se^{2-} anions like in a cubic close packed structure. It must be mentioned that alternating signs of the translation vector yield to the arrangement AB as realised in hexagonal close packed structures. To achieve the chalcopyrite structure of α-CuInSe2 the ABC stacking is required. Any deviation introduces to stacking faults along the ⟨112⟩ direction of α CuInSe2.
4. So far the ions are ordered as $(Cu–Se)_3$–$(In–Se)_3$ along ⟨001⟩. To obtain the alternate order of the cations as realised along ⟨110⟩ in α-CuInSe2 cation exchanges across the {001} contact surfaces are necessary (Fig. 10c). After this step the ion sequence $(Cu–Se–In–Se)_3$ is achieved.

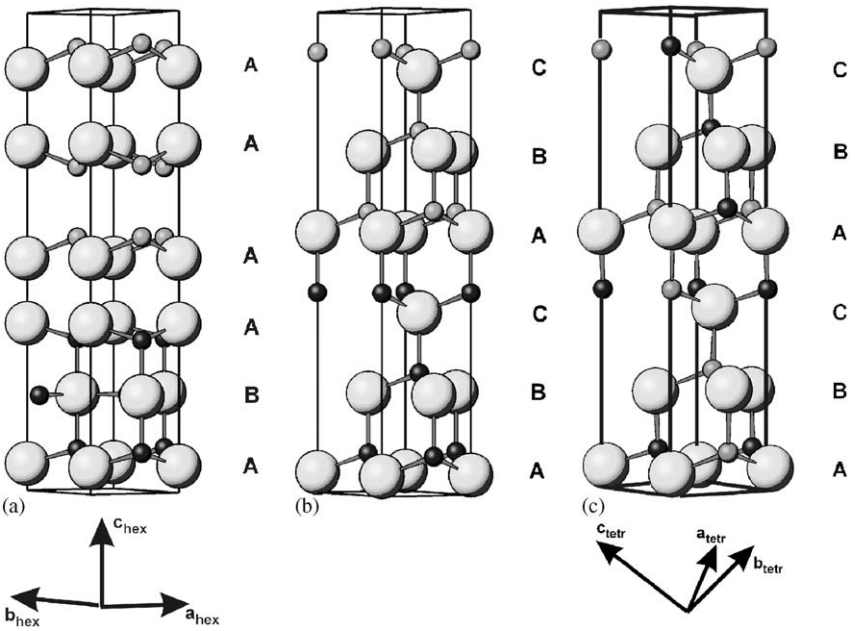

Fig. 10. Schematic drawing of reaction A viewing perpendicular to ⟨001⟩ Cu^+: dark small balls, In^{2+} and In^{3+}: grey small balls, Se^- and Se^{2-}: large bright balls.

A slight rearrangement of the Se^{2-} anions from $x(Se) = \frac{1}{4}$ to $x(Se) = 0.224$ (referring to the tetragonal setting) results in the chalcopyrite structure (Fig. 5a).

The whole transformation into α-$CuInSe_2$ is completed by these four steps. As we started with epitaxy of two {001} facets containing plane selenium hexagons we expect the {112} lattice plane of $CuInSe_2$ to be formed. In this case the Se^{2-} anions are already located almost in their correct positions, the chalcopyrite crystal structure is realised by the correct ordering of the cations. The maximum change in atomic distances in the {001} plane of γ-CuSe compared with those in the {112} plane of α-$CuInSe_2$ is just 30‰ (Table 7).

We summarise that reaction A is facilitated by epitaxy followed by a subsequent redox reaction breaking up covalent bonds allowing the cation exchange. The most complicated step is the arrangement of the cations necessary to achieve tetrahedral coordination for the Cu (2*d*) and Se (2*c*) atoms in γ-CuSe.

Experimental proof: Reaction A occurs when tempering SEL above the melting point of selenium at 221 °C [5], which is at the same time the minimum temperature for the formation of the starting compounds γ-CuSe and InSe. The reaction was also observed during isothermal annealing a layer stack of γ-CuSe on top of InSe [5]. This agrees well to experiments [59], in which the formation of α-$CuInSe_2$ on the expense of γ-CuSe was observed when annealing a bilayer stack of γ-CuSe deposited on X-ray amorphous InSe. The activation energy was determined to $E_{act}(A) = 66\,kJ/mol$ [59]. For a bilayer stack of crystalline phases we could identify a one-dimensional growth process limited by diffusion with an activation energy of $E_{act}(A) = 128\,kJ/mol$ [60].

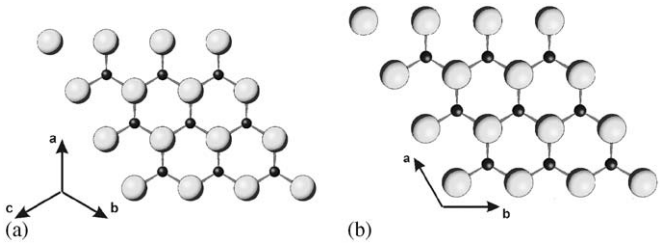

Fig. 11. Possible planes suitable for epitaxy: (a) Cu_2Se {111}, (b) InSe {001} Cu^+ and In^{2+} dark, Se^{2-} bright balls.

4.2. *Reaction B:* $\frac{1}{2}\beta$-Cu_2Se+InSe+$\frac{1}{2}$ Se (liq.) → $CuInSe_2$

This reaction can take place above 221 °C, after selenium has molten. The reaction is a solid–solid–liquid reaction. The best match of the lattices of β-Cu_2Se and InSe is achieved by epitaxy of the InSe {001} with the β-Cu_2Se {111} plane. As stated in Section 3, these planes are expected to occur as crystal facets according to the BNDH law.

The anion–anion and cation–cation distances in the {111} plane of the zincblende sublattice of β-Cu_2Se are just 20‰ larger than the corresponding distances in 2H–InSe (Table 7). The reaction is described most easily by the following steps:

1. β-Cu_2Se and InSe crystals connect epitaxially at one possible facet (Fig. 11). Due to symmetric equivalence

this can take place at up to eight {111} facets of the β-Cu_2Se crystal simultaneously.

2. At the interface of the epitaxially connected crystals with the selenium melt the following redox reaction with a selenium chain is likely to occur:

$$[In-In]^{4+}{}_{\text{in InSe}} + [Se_n]^0{}_{\text{in the melt}} \rightarrow 2\ In^{3+} + Se^{2-} + [Se_{n-1}]^0{}_{\text{in the melt}}.$$

In this case the indium dication is embedded in the InSe crystal structure whereas the selenium atom must be separated from selenium chains present in the melt. The β-Cu_2Se crystal is known to be electron conductive. Hence, we expect the $[In_2]^{4+}$ cation to be oxidised being located at the interface of the β-Cu_2Se and the InSe crystal, whereas the reduction of selenium occurs at the surface of the β-Cu_2Se crystal. To maintain charge neutrality within the β-Cu_2Se crystal two electrons have to diffuse through the β-Cu_2Se crystal towards that surface in contact with the selenium melt. Consequently, after its reduction the Se^{2-} anion will be bonded to the surface of the β-Cu_2Se crystal. Since no epitaxial relation needs to be satisfied for single ions on surfaces, any surface {*hkl*} of the β-Cu_2Se crystal is sufficient for this. Due to the anisotropic ion conductivity of β-Cu_2Se the {111} facets are the most prominent planes on which the Se^{2-} anions can be adsorbed. This reaction mechanism supported by the ambipolar ion conductivity of the β-Cu_2Se crystal implies the interesting aspect, that the β-Cu_2Se crystal increases its size in at least two different directions: At first it grows perpendicular to the {111} facet due to the epitaxial contact with an InSe crystal. Second, it grows at those facets where Se^{2-} anions are adsorbed (Fig. 12a).

3. Due to the complete oxidation the In^{3+} cations will prefer to coordinate tetrahedrally with Se^{2-} anions. This is achieved by exchange of In^{3+} with Cu^+ cations. In^{3+} cations from the indium double layers of InSe will diffuse into the crystal structure of β-Cu_2Se and Cu^+ cations will diffuse between the selenium double layers in the InSe structure (Fig. 12b). The diffusion of In^{3+} in the ion conducting β-Cu_2Se phase was found to approach a value typical for diffusion in liquids [61]. However, this is a self-inhibiting process as the β-Cu_2Se crystal is gradually changed into α-$CuInSe_2$ where no ion conductivity favours the cation diffusion any more. Therefore, we expect the reaction rate of this process to decrease in time once initiated. This is due to the increasing diffusion length through the forming α-$CuInSe_2$ interface. Thus there are two steps: the formation of an α-$CuInSe_2$ layer, and a diffusion limited growth. The cation diffusion within InSe is limited as well, however, since we can expect small crystal platelets as the reaction partners, which start to dissolve into single layers due to oxidation. Thus, the diffusion length along the $\langle 001 \rangle$ direction is short in comparison. As in reaction A there exist several possibilities for the Se^{2-} anion arrangement. The β-Cu_2Se crystal structure is already ordered like ABC along the $\langle 111 \rangle$ axes. However, the InSe structure needs to be rearranged. A perfect ABC ordering of the Se^{2-} anions is realised along the $\langle 112 \rangle$ directions in the chalcopyrite crystal structure of α-$CuInSe_2$.

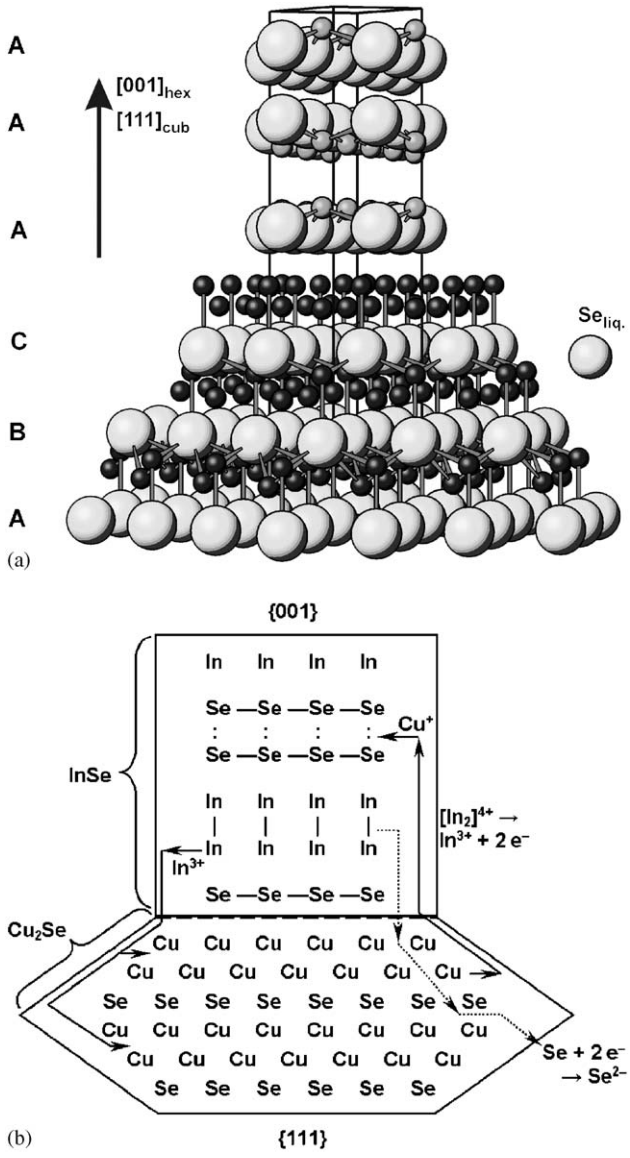

Fig. 12. Illustration of reaction B. In (a) $1\frac{1}{2}$ motifs of InSe have connected to one of the {111} facets of β-Cu_2Se. The unit cell of InSe is drawn as a guideline for the eye, only. The cation exchange is initiated by a redox reaction (b). Note that no Se^{2-} anion transport is required. Cu^+ dark, In^{2+} bright small balls; Se^{2-} large bright balls.

For reaction B to proceed we exploit epitaxy of β-Cu_2Se {111} with InSe {001} lattice planes, both containing plane selenium hexagons. Therefore, we assume the {112} lattice planes of the chalcopyrite structure to be formed from this reaction.

The ambipolar ion conductivity of β-Cu_2Se allows the cation exchange necessary to form the tetragonal α-phase of $CuInSe_2$. It further enables quick diffusion compared to

reaction A (cf. Section 4.1). Since the zincblende sublattice of β-Cu_2Se provides the template structure of the chalcopyrite, large β-Cu_2Se crystals will inevitably result in large grains of α-$CuInSe_2$. Although being a simultaneous reaction of three reaction partners, the argument that reaction B is improbable as it requires a three-body interaction cannot be applied here. After the contact of β-Cu_2Se with InSe, the reduction of selenium need not have to occur at the same interface. To provide a quick reaction the β-Cu_2Se crystal only needs to be surrounded by the selenium melt and InSe crystal platelets. The melt steadily provides contact with selenium and, moreover, supports the diffusion of InSe platelets towards the β-Cu_2Se crystals.

Experimental proof: Reaction B was identified during annealing of copper indium layers in H_2Se at 400 °C [62]. Later, the reaction rates at different temperatures and the activation energy $E_{act}(B) = 25\,kJ/mol$ was determined [63]. The reaction equation was shown to be valid also when replacing H_2Se by elemental selenium [64]. When tempering in a low amount of selenium, the reaction remains incomplete, which can be recognised from the residual solid-state educts [42].

In our group reaction B was observed to take place during annealing SEL [4,5]. Both authors describe the influence of sodium doping on the reaction temperature. When reaction B is preferred rather than reaction A, the processed absorber will consist of large $CuInSe_2$ grains [5]. Consequently, we suppose this to be a beneficial formation reaction in means of reducing the number of grain boundaries in the absorber material. Furthermore, we have proven reaction B to take place during annealing of a bilayer consisting of γ-CuSe on top of InSe [5].

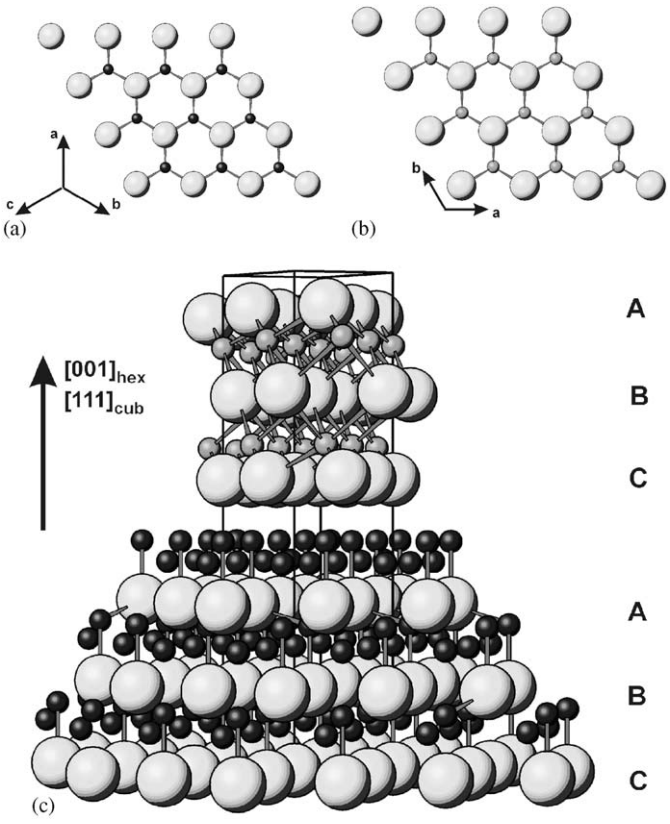

Fig. 13. Possible planes suitable for epitaxy: (a) Cu_2Se {111}, (b) β-In_2Se_3 {001} Illustration of the layer sequence after the epitaxial connection of one β-In_2Se_3 motif with crystal structure β-Cu_2Se. The unit cell edges of the hexagonal β-In_2Se_3 structure are inserted as a guideline for the eye. Cu^+ dark, In^{3+} bright small balls; Se^{2-} large bright balls.

4.3. Reaction C: $\frac{1}{2}\,\beta$-$Cu_2Se + \frac{1}{2}\,In_2Se_3 \rightarrow CuInSe_2$

This reaction differs from the two described above, as no redox reaction is involved to break up the Se–Se bonds facilitating the recoordination of the cations. Since there exist two modifications of In_2Se_3 in the relevant temperature range, we have to discuss the reaction with both, β- and γ-In_2Se_3 as reactants, separately. The chemical reaction involving β-In_2Se_3 will be denoted as Cβ, that with γ-In_2Se_3 as starting compound is abbreviated by Cγ in the following.

4.3.1. Reaction Cβ: $\frac{1}{2}\,\beta$-$Cu_2Se + \frac{1}{2}\,\beta$-$In_2Se_3 \rightarrow CuInSe_2$

When searching for epitaxial relations for this reaction we observe a good agreement of the atomic distances in the {001} plane of β-In_2Se_3 and the {111} plane of β-Cu_2Se (Fig. 13a,b) with a lattice misfit of only 20‰ (Table 7). These facets are likely to form according to the BNDH law. Since both epitaxial lattice planes contain planes centred selenium hexagons we expect the formation of {112} lattice planes of α-$CuInSe_2$. These layers are stacked in the sequence ABC. This stacking sequence of the Se^{2-} anions is already realised in the crystal structure of β-Cu_2Se as well as within the motif of β-In_2Se_3 (Fig. 13c). To obtain a perfect ABC arrangement for more than one motif of β-In_2Se_3, however, the β-In_2Se_3 motifs must undergo a translation of $(\frac{1}{3}, \frac{2}{3}, 0)$ between two adjacent motifs. Additionally, the In^{3+} cations must change into tetrahedral coordination. As a result of these steps stacking faults are probable to be introduced into the chalcopyrite crystal structure of α-$CuInSe_2$.

For the final ordering of the chalcopyrite, cation exchange between the educts is required. The only diffusion direction which seems easily possible is in between the motifs perpendicular to the $\langle 001 \rangle$ direction of β-In_2Se_3, where two Se^{2-} anions are juxtaposed to each other. Cu^+ cations can intrude between the motifs of the β-In_2Se_3 crystal structure by breaking up the van-der-Waals Se–Se bonds. Unfortunately, this possibility of indiffusion is perpendicular to the epitaxial {001} lattice planes. For this reason we conclude that despite the existence of an epitaxial relation the consecutive exchange of Cu^+ and In^{3+} cations will be a difficult and thus a slow reaction step, which is driven by the concentration gradient of the different cations. Thus, reaction Cβ will be a slow solid-state reaction requiring a higher activation energy than reaction B.

Experimental proof: When annealing SEL β-Cu_2Se and β-In_2Se_3 formed as intermediate products further reacting

with each other at 400 °C and above forming α-$CuInSe_2$ [65]. The reaction was completed at 450 °C after 1 min.

4.3.2. Reaction Cγ: $\frac{1}{2}$ β-Cu_2Se+$\frac{1}{2}$ γ-In_2Se_3 → α-$CuInSe_2$

There are two different epitaxial relations, involving either the {100}, or the {001} facets of γ-In_2Se_3. The first possibility seems to be more important and has been confirmed experimentally without doubt.

(a) *Epitaxy on the {100} facets of γ-In_2Se_3:* The {100} planes of γ-In_2Se_3 contain buckled, distorted Se^{2-} hexagons (Fig. 14). They are centred as in the {111} planes of β-Cu_2Se with a misfit of 12‰ considering the averaged distance value of the Se^{2-} anions. Neglecting the distortion, the whole Se^{2-} anion sublattice fulfils the epitaxial relation with the anion sublattice of β-Cu_2Se. As there are six symmetrically equivalent {100} planes, epitaxy is always ensured with one of the eight {111} facets of β-Cu_2Se. This is especially important for randomly oriented crystals growing on a flat substrate where material can be supplied perpendicular to the surface, only. The Se^{2-} anions are arranged in corrugated distorted centred hexagons on the {100} facets of γ-In_2Se_3 like on the {110}/{102} lattice planes of α-$CuInSe_2$. This is the reason why this reaction does not result in the formation of {112} lattice planes of α-$CuInSe_2$ as all other reactions described so far, rather in the {110}/{102} facets of α-$CuInSe_2$. The formation of the latter facets is not expected in equilibrium crystal growth conditions, as given by the BNDH law.

This reaction requires extensive ion rearrangement, since there exits no simple stacking sequence of the Se^{2-} anions planes in γ-In_2Se_3 perpendicular to the {100} lattice plane like AB or ABC.

(b) *Epitaxy on the {001} facets of γ-In_2Se_3:* The {001} lattice planes of γ-In_2Se_3 contain distorted Se^{2-} hexagons fitting to the {111} planes of β-Cu_2Se. The lattice misfit equals zero within the accuracy of the average distance values of Table 7. The epitaxy of the anion lattice works only for every second Se^{2-} anion of the (00−1), and only for each fourth Se^{2-} anion of the (001) planes of γ-In_2Se_3 (Fig. 15). For this reason the prerequisites for epitaxy are not ideal. In particular, the growth on the (001) lattice plane of γ-In_2Se_3 must be regarded to be more improbable than epitaxy on the (00−1) plane. Additionally, the {001} facets of γ-In_2Se_3 are not expected to form before the tenth place on the ranking given by the BNDH law. If, nevertheless, epitaxy of the (00−1) facet of γ-In_2Se_3 with one of the {111} facets of β-Cu_2Se occurs, we can expect the formation of {112} lattice planes of α-$CuInSe_2$, since we can regard both Se^{2-} anion lattice planes to be plane. To get the ABC stacking sequence of the Se^{2-} anions as realised in the chalcopyrite structure and in β-Cu_2Se, the Se^{2-} anions of the γ-In_2Se_3 structure, not having a simple stacking sequence, need to be rearranged.

According to the BNDH law, we forecast that reaction Cγ is realised by epitaxy of {001} lattice planes of γ-In_2Se_3 with {111} planes of β-Cu_2Se. However, independent for which of the two epitaxial mechanisms we decide to initiate reaction Cγ, the initial epitaxial reaction step must be followed by cation exchange in between these two compounds. Because of the dense network of the three dimensionally interconnected structure of γ-In_2Se_3 we

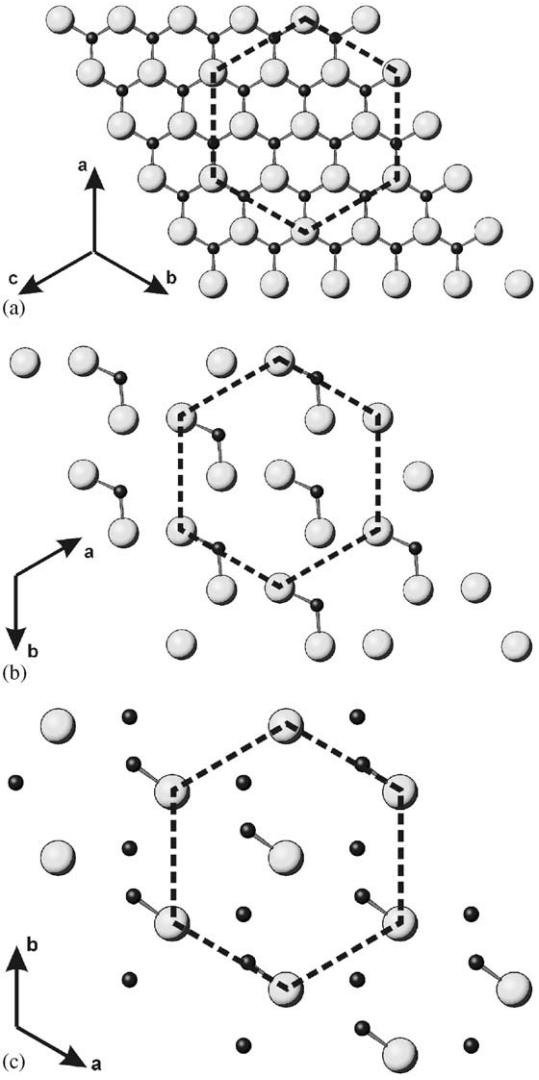

Fig. 15. Epitaxial relation between (a) β-Cu_2Se {111}, (b) γ-In_2Se_3 (00−1) and γ-In_2Se_3 (001) (c). The marked hexagon in (a), (b) and (c) contains eight, four and two Se^{2-} anions, respectively. Epitaxy with the {111} facet of β-Cu_2Se is fulfilled for every second Se^{2-} anion of the (00−1) lattice plane and for every fourth Se^{2-} anion of the (001) plane of γ-In_2Se_3 only. Thus, we expect the (00−1) facet to preferentially take part in this reaction. Cu^+ and In^{3+} dark, Se^{2-} bright balls.

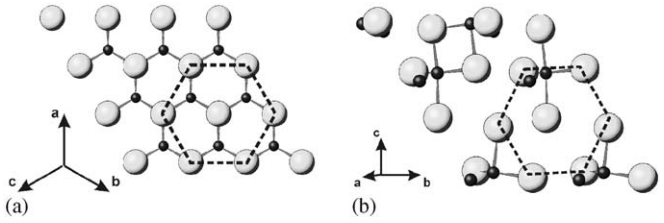

Fig. 14. Epitaxial planes for reaction mechanism b: (a) β-Cu_2Se {111} and (b) γ-In_2Se_3 {100}. Cu^+ and In^{3+} dark, Se^{2-} bright balls.

expect this modification not to be a beneficial reaction partner for β-Cu_2Se. This is the reason, why reaction Cγ requires a relatively high temperature to overcome the activation energy and secondly, it is slow compared to reaction B.

Experimental proof: Reaction Cγ was identified by us with real-time XRD experiments during annealing a bilayer of γ-CuSe on InSe. It takes place slowly, beginning not below 425 °C [5].

When γ-In_2Se_3 was grown during the first stage of PVD such, that its $\langle 001 \rangle$ axis was oriented parallel to the substrate, the growth of plate like crystals of α-CuIn(Ga)Se_2 with their {110}/{102} facets parallel to the substrate has been found [9]. This is in perfect agreement with our model presented above. An orientation of γ-In_2Se_3 with its $\langle 001 \rangle$ axis lying parallel on the substrate means that three of the six symmetrically equivalent {100} facets are pointing upwards from the surface of the substrate. During the second stage of PVD the elements copper and selenium are offered and the {111} lattice planes of just formed β-Cu_2Se can epitaxially connect to the {100} facets of γ-In_2Se_3. As a consequence the compound α-CuIn(Ga)Se_2 grows with its {110}/{102} lattice planes approximately parallel to the substrate, which is seen in TEM pictures [66]. TEM further proves that these platelets are almost free of defects compared to {112} platelets [66]. It was also shown, that the 110/102 texture of α-CuIn(Ga)Se_2 is more pronounced for increased selenium excess [67] during the first stage, which confirms that γ- rather than β-In_2Se_3 (which is a slightly selenium deficient compound [34]) is the reactant for the reaction. The formation of {110}/{102} facets of α-CuIn(Ga)Se_2 during PVD proves that a mechanism other than equilibrium crystal growth has occurred, since these facets are improbable to form according to the BNDH law. The occurrence of the {110}/{102} facets is a consequence of the epitaxially initiated solid-state reaction.

The experiments above are well complemented by the finding, that γ-In_2Se_3 grown with its $\langle 001 \rangle$ axis oriented perpendicularly to the substrate resulted in the formation 112 textured α-CuIn(Ga)Se_2 during two stage PVD [68]. Under such experimental conditions the $\langle 100 \rangle$ directions of the γ-In_2Se_3 crystals are parallel to the substrate where epitaxial growth on the {100} facets cannot proceed. Instead the only remaining possibility for epitaxy is to use the (00−1) lattice plane of γ-In_2Se_3 resulting in the formation of {112} lattice planes of $CuInSe_2$.

Finally, the compound β-$CuInSe_2$ was shown to form by annealing of two ingots in contact with each other [61]. The ingots were synthesised from Cu_2Se and In_2Se_3 powders. Unfortunately, no phase is specified for the latter compound; we suppose γ-In_2Se_3 to be the most probable in this base. After annealing at 550 °C the high temperature phase β-$CuInSe_2$ was stabilised down to room temperature due to epitaxy with β-Cu_2Se.

4.4. Reaction D: $\frac{1}{2}\beta$-$Cu_2Se+\frac{1}{2}\alpha$-$Ga_2Se_3 \rightarrow \alpha$-$CuGaSe_2$

This reaction describes a separate reaction path for the Ga^{3+} cations in a quaternary precursor, as gallium was not found to take part in reactions A–C. Similarly to reaction C this is no redox reaction. As both starting compounds are no layered structures, the concept of subunits cannot be applied here, neither. The initiating step is epitaxy between the {111} facets of β-Cu_2Se and the {010} facets of α-Ga_2Se_3 (Fig. 16a,b) with a lattice misfit of 59‰. The stacking sequence of the Se^{2-} anions in α-Ga_2Se_3 along $\langle 010 \rangle$ is AB unlike to ABC as realised in cubic β-Cu_2Se. Therefore, epitaxy must be followed by cation exchange and rearrangement of the Se^{2-} anions in α-Ga_2Se_3. Due to the corrugated Se^{2-} hexagons extending over two adjacent {010} lattice planes of α-Ga_2Se_3 we expect the formation of {110}/{102} planes of α-$CuGaSe_2$, which are corrugated, too.

It is worthwhile to note that the β-phase of Ga_2Se_3 becomes stable above 730 °C. The crystal structures of β-Cu_2Se and β-Ga_2Se_3 are isostructural to each other (except for vacancies). This means that epitaxy is possible on any two identical lattice plane {*hkl*} for arbitrary *h*, *k*, *l*. This special case of epitaxy is called topotaxy. As crystals of β-Cu_2Se offer only {111} facets, the reaction will exploit epitaxy of the {111} planes of both structures with a misfit of 76‰ (Fig. 16a,c). The Se^{2-} anions are arranged in layers stacked according to ABC in both crystal structures of the educts, which is an optimal prerequisite to avoid stacking faults along the $\langle 112 \rangle$ directions in α-$CuInSe_2$. Due to the cation conductivity of both reactants, the cation exchange can easily begin and continue in the volume of both structures. In other words, this solid-state reaction is achieved by interdiffusion of cations between the topotactic

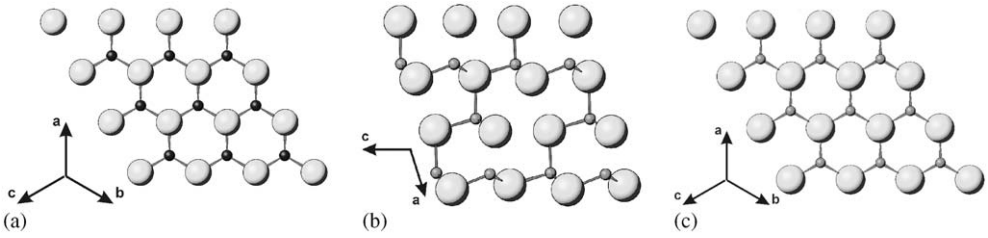

Fig. 16. Epitaxial planes of the reaction partners: (a) Cu_2Se {111}, (b) corrugated Se^{2-} hexagons in α-Ga_2Se_3 {010}, c) β-Ga_2Se_3 {111} Cu^+: dark small balls, Ga^{3+}: middle grey small balls, Se^{2-}: large bright balls.

crystal structures. However, as in the case of reaction B this is a self-inhibiting process, as the resulting structure of α-$CuGaSe_2$ does not provide cation conductivity, any more.

Experimental proof: We have experimentally observed reaction D to begin at 400 °C [5] initiated by the crystallisation of Ga_2Se_3. Due to the high similarity between the crystal structures of the α- and the β-phase, we could not distinguish these phases by their powder diffraction patterns. However, according to the phase diagram [19] we have to expect α-Ga_2Se_3 at 400 °C rather than β-Ga_2Se_3. Since α-Ga_2Se_3 must have been formed from the metallic precursor, we assume that this compound has been present below this temperature already, most possibly X-ray amorphous. The formation of α-$CuGaSe_2$ starts exactly with the appearance of α-Ga_2Se_3, never before. This obviously coincides with the development of the necessary {010} crystal facets of α-Ga_2Se_3.

In a recent thermal analysis we have proven that the exothermic heat flow of reaction D splits up into two signals [60]. From these data we have calculated the activation energies of both partial reactions to be 148 and 129 kJ/mol, respectively.

Reaction D was also observed during the one and two stage PVD process above 500 °C and the mechanism of topotaxy between β-Cu_2Se and α-$CuGaSe_2$ was proposed [69]. The starting compounds for this reaction have been identified after interrupting the annealing process of a $CuIn_{0.75}Ga_{0.25}$ alloy at 400 °C [42].

4.5. Reaction E: $\frac{3}{4}$α-$CuInSe_2$+$\frac{1}{4}$α-$CuGaSe_2$ → α-$CuIn_{0.75}Ga_{0.25}Se_2$

This reaction is an example for a pure diffusion reaction of two topotactical structures. The gallium content of 25% in the quaternary chalcopyrite serves as example, only. The reaction mechanism is valid for the whole $CuIn_{1-x}Ga_xSe_2$ solid solution range. The interdiffusion of the ternaries will be driven by the increase of the entropy in the quaternary compound compared to the ternary chalcopyrites. The lattice misfit is only 43‰ for Cu–Cu and Se–Se distances, valid for any facet {*hkl*}. For this pure diffusion reaction E we cannot exploit any cation conductivity supporting the diffusion. Hence, we expect the diffusion current to be proportional to the concentration gradient for each two facets being in epitaxial contact. This is mathematically formulated as Fick's second law of diffusion:

$$dC/dt = Dd^2C/dL^2, \quad (1)$$

where L is the distance form the interface. Eq. (2) is an approximate solution for Eq. (1) [70]:

$$C(L) = \tfrac{1}{2}C(L=0)[1 - \mathrm{erf}\{L/(4Dt)^{1/2}\}]. \quad (2)$$

The input parameters of this model are the Ga^{3+} cation concentration C, defined as the ratio of concentrations $[Ga^{3+}]/([In^{3+}]+[Ga^{3+}])$, and the diffusivity D of Ga^{3+} cations in $CuIn_{1-x}Ga_xSe_2$. The diffusivity D does not have to be constant in time. It can for example decrease during the interdiffusion like $D \sim t^{-\alpha}$ with $\alpha > 0$ [70]. The qualitative Ga^{3+} cation concentration $C(L)$ is expected to obey a distribution perpendicular to the connected facets given by the error function $\mathrm{erf}\{L/(4Dt)^{1/2}\}$. Thus, the reaction time t will depend on the size of the crystals (or the diffusion length L, respectively), the gallium concentration C and lateral homogeneity dC/dL desired.

Experimental proof: We have shown reaction E to take place as soon as reaction D has begun to form α-$CuGaSe_2$ [5]. Once initiated, the reaction rate decreases exponential like in time, as expected, and takes about 1.5 min. Moreover, we have experimentally shown that the diffusion rate D is reduced, if the precursor contains a sodium dopant (cf. Section 4.9). In this case the reaction may remain incomplete. The diffusion rate of Ga^{3+} within α-$CuInSe_2$ and of In^{3+} within α-$CuGaSe_2$ was found to be similar [71]. The authors concluded that the diffusing atoms are moving via vacant lattice sites through the crystal. Taking the experimentally determined values for the diffusivity of Ga^{3+} into $CuInSe_2$ at 725 °C [72] we can estimate the duration of reaction E. With $D = 5.5 \times 10^{-13}\,cm^2/s$, $L = 10^{-5}\,cm$ as diffusion length and $\alpha = 1$, the argument of the error function becomes unity at $t = 45\,s$, which is the typical reaction time. This is double as fast as experimentally observed, which is mainly due to the different reaction temperatures.

4.6. Reactions not observed during annealing of SEL

Except for the five main reactions discussed above there is a variety of additional binary reactions in the copper–indium–gallium–selenium system one can think of. We give just four examples here to explain the main ideas why these reactions are unlikely to occur.

4.6.1. $CuSe_2$+$\frac{1}{4}In_4Se_3$–$\frac{3}{4}Se(liq.)$ → α-$CuInSe_2$

Even with a high phase content of In_4Se_3 and $CuSe_2$ directly after the selenisation of a copper–indium precursor, this reaction was not observed [5]. The crystal structures of both compounds consist of stable networks, not of layered structures as in the case of γ-CuSe or InSe. Principally these networks could be broken up due to the following redox reaction, destroying the In–In bonds within the polycation $[In_3]^{5+}$ and the Se–Se bonds of the polyselenide anion $[Se_4]^{2-}$:

$$2[Se_4]^{2-}_{\text{in } CuSe_2} + (In^+ + [In_3]^{5+})_{\text{in } In_4Se_3} - 3[Se]^0_{\text{in the melt}} \rightarrow (4In^{3+} + 5Se^{2-})_{\text{in } CuInSe_2}.$$

Nevertheless, this reaction is not observed experimentally. We assume that the reason therefore, is the missing epitaxial relation for both educt structures to get connected as a prerequisite for a quick electron transfer. Instead, we have observed a slow redox reaction avoiding the total oxidation of In^+ and the complete reduction to Se^{2-}. This selenium exchange reaction (see Section 4.6.2) can be understood as an intermediate step. Having reached this

state, the compounds γ-CuSe and InSe allow reaction A to begin with the formation of α-$CuInSe_2$.

4.6.2. Reactions involving In_4Se_3, In_6Se_7 or $CuSe_2$

There exist no epitaxial relations between In_4Se_3 and In_6Se_7 and any of the copper selenides and of $CuSe_2$ with any of the indium or gallium selenides. This is mainly due to the relatively complex crystal structure of the title compounds. Thus, we expect any reaction involving the title compounds as reactants to be slow, despite the fact that the electron transfer involved in such redox reactions would dismount the crystal structures of the reactants. Indeed, the reaction

$$CuSe_2 + In_4Se_3 \rightarrow \gamma\text{-}CuSe + 4InSe$$

was found to proceed slowly in comparison to epitaxially promoted solid-state reactions [5].

4.6.3. γ-$CuSe + \frac{1}{2}In_2Se_3 - \frac{1}{2}Se \rightarrow \alpha$-$CuInSe_2$

In this case there are ideal prerequisites for epitaxy, since the {001} facets of γ-CuSe fit to the {001} planes of β-In_2Se_3 (Fig. 13b) as well as to the {100} (Fig. 14b) and to the {001} planes of γ-In_2Se_3 (Fig. 15b,c). Contrary to reactions Cβ and Cγ (cf. Section 4.3) there is no cation conductive starting compound involved, why we must expect a slow interdiffusion reaction. Additionally, the selenium in γ-CuSe must disproportionate according to

$$2\gamma\text{-}CuSe \rightarrow \beta\text{-}Cu_2Se + Se$$

We expect β-In_2Se_3 rather than γ-In_2Se_3 to be the more advantageous reaction partner due to its van-der-Waal bonds. In a reaction of γ-CuSe with β-In_2Se_3 the cation can diffuse perpendicular to the $\langle 001 \rangle$ direction of both structures and selenium can be released through these gaps.

When annealing SEL, none of both reactions is observed in practice [5]. This is due to the fact that the formation of In_2Se_3 is suppressed due to the formation of α-$CuInSe_2$ via reactions A or B, both consuming InSe. However, annealing a bilayer of γ-CuSe on γ-In_2Se_3 facilitated to observe this reaction [73] above 230 °C. The reaction is controlled by one-dimensional diffusion through the interface. The activation energy is determined as 162 kJ/mol.

4.6.4. γ-$CuSe + GaSe \rightarrow \alpha$-$CuGaSe_2$

This reaction is expected to take place due to the same arguments as given above for reaction A, since GaSe and InSe are isostructural with a misfit of 60‰. The reason, why this reaction is actually not observed when tempering precursors containing gallium and indium simultaneously is due to chemical differences between gallium and indium. As explained in Section 3.2.1 we expect gallium from the metallic precusor to be selenised to α-Ga_2Se_3 whereas indium remains in a lower oxidation state. The oxidation to Ga^{3+} can take place either directly from elemental gallium, or via GaSe by a rapid further selenisation of GaSe to α-Ga_2Se_3 during annealing SEL.

Assuming that GaSe is intermediately formed during the selenisation of SEL, the reaction proposed above can of course take place. We even expect this reaction path to be taken in SEL precursors consisting of copper, gallium and selenium without indium or for bilayers of γ-CuSe and GaSe. However, the same reasons as given for reaction A let us expect the reaction speed to be low. If the selenisation proceeds further producing α-Ga_2Se_3 reaction D can start.

4.7. Overview

All epitaxially promoted reactions are summarised in Table 8. The reactions are ordered by their bonding type beginning with the weakest interaction. For all reactions the epitaxial planes of the educts and the corresponding lattice plane in the chalcopyrite structure are given. All reactions require epitaxy as initiating step. Only those planes likely to form crystal facets according to the BNDH law are considered here. In two cases the reactants have an infinite number of possible planes in common, or, in other words, this reactions are topotaxial. In practice, however, the number of capable facets is either limited due to ion conductivity (β-Ga_2Se_3), or by the BNDH law (rct. E). From the different mechanisms involved we estimate relative reaction speeds.

4.8. Summary of essential reaction steps

From the reactions described above we recognise essential prerequisites promoting the solid-state reactions involved in the chalcopyrite formation. We expect that an epitaxially promoted solid-state reaction will start at lower temperature and thus proceed faster in an annealing process than a general solid-state reaction not taking advantage of epitaxy. This has been recognised for the spinell formation by solid-state reaction of NiO with different single crystal facets of α-Al_2O_3 [74]. The epitaxial reaction of NiO-{111} with the {110} facet of α-Al_2O_3 containing distorted buckled oxygen hexagons in two adjacent lattice planes has been found to have the lowest activation energy. This is explained by assuming corrugated facets to possess a lower bond strength which supports epitaxy [75]. Such corrugated crystal facets are involved in the four reactions marked by footnote 'd') in Table 8.

In the following we assume to start with a mixture of two solids having developed crystals large enough that their surface consists of typical facets, which are predicted by the BNDH law.

1. First of all, an *epitaxial* relation is required to provide contact of the two different crystals. The required facets have to be formed for both crystals. If no epitaxially related facets can be found, the reaction is suppressed. This is even true, if the reaction was exothermic, as discussed in Section 4.6.1. An epitaxial connection is sufficient for the ion diffusion to start between the crystals.

Table 8
Summary of described reactions involving epitaxy ordered by ionicity of the educts

	Reaction	Bond types[a]	Epitaxial planes	Mechanisms[b]	Reaction speed	Reaction observed[c]
(A)	γ-CuSe	Cov/vdW	{0 0 1}	vdW-epitaxy, redox rct.	Slow	A of SEL
	+ 2H/3R-InSe	Cov/vdW	{0 0 1}			A of BL
	$\rightarrow \alpha$-$CuInSe_2$	Ion	{1 1 2}			IA of BL
	γ-CuSe	Cov/vdW	{0 0 1}	vdW-epitaxy, redox rct.	Slow	No
	+ 2H/3R-GaSe	Cov/vdW	{0 0 1}			
	$\rightarrow \alpha$-$CuGaSe_2$	Ion	{1 1 2}			
	2γ-CuSe	Cov/vdW	{0 0 1}	Epitaxy	Slow	No
	+ β-In_2Se_3	Ion/vdW	{0 0 1}			
	−Se(liq.)	Cov	—			
	$\rightarrow 2\alpha$-$CuInSe_2$	Ion	{1 1 2}			
	2γ-CuSe	Cov/vdW	{0 0 1}	Epitaxy	Slow	A of BL
	+ γ-In_2Se_3	Ion	{1 0 0}			
	−Se(liq.)	Cov	—			
	$\rightarrow 2\alpha$-$CuInSe_2$	Ion	{1 1 0}/{1 0 2}[d]			
	2γ-CuSe	Cov/vdW	{0 0 1}	Epitaxy	Slow	No
	+ α-Ga_2Se_3	Ion	{0 1 0}			
	−Se(liq.)	Cov	—			
	$\rightarrow 2\alpha$-$CuInSe_2$	Ion	{1 1 0}/{1 0 2}[d]			
(B)	β-Cu_2Se	Ion	{1 1 1}	Epitaxy, redox rct., ion cond.	Fast	A of SEL
	+ 2 2H/3R-InSe	Cov/vdW	{0 0 1}			A of BL
	+ Se(liq.)	Cov	—			
	$\rightarrow 2$ α-$CuInSe_2$	Ion	{1 1 2}			
	β-Cu_2Se	Ion	{1 1 1}	Epitaxy, redox rct., ion cond.	Fast	No
	+ 2 2H/3R-GaSe	Cov/vdW	{0 0 1}			
	+ Se(liq.)	Cov	—			
	$\rightarrow 2$ α-$CuInSe_2$	Ion	{1 1 2}			
(Cβ)	β-Cu_2Se	Ion	{1 1 1}	Epitaxy, ion cond.	Slow	IA of SEL
	+ β-In_2Se_3	Ion/vdW	{0 0 1}			
	$\rightarrow 2$ α-$CuInSe_2$	Ion	{1 1 2}			
(Cγ)	β-Cu_2Se	Ion	{1 1 1}	Epitaxy, ion cond.	Slow	A of BL
	+ γ-In_2Se_3	Ion	{1 0 0}			PVD
	$\rightarrow 2$ α-$CuInSe_2$	Ion	{1 1 0}/{1 0 2}[d]			IA of BL
(D)	β-Cu_2Se	Ion	{1 1 1}	Epitaxy, ion cond.	Slow	A of SEL
	+ α-Ga_2Se_3	Ion	{0 1 0}			A of BL
	$\rightarrow 2$ α-$CuGaSe_2$	Ion	{1 1 0}/{1 0 2}[d]			PVD
	β-Cu_2Se	Ion	{1 1 1}	Topotaxy, ion cond.	Fast[e]	No
	+ β-Ga_2Se_3	Ion	{1 1 1}			
	$\rightarrow 2$ α-$CuGaSe_2$	Ion	{1 1 2}			
(E)	3 $CuInSe_2$	Ion	{h k l}	Topotaxy	Slow	A of SEL
	+ $CuGaSe_2$	Ion	{h k l}			
	$\rightarrow 4$ $CuIn_{0.75}Ga_{0.25}Se_2$	Ion	{h k l} for arbitrary h, k, l			

[a] vdW: van-der-Waals, Cov: covalent, Ion: ionic bonds.
[b] vdW-epitaxy: van-der-Waals epitaxy, redox rct.: redox reaction, ion cond.: ionic conductivity.
[c] A: annealing, IA: isothermal annealing, SEL stacked elemental layers, BL: bilayers.
[d] We consider the planes {1 1 0} and {1 0 2} being symmetrically equivalent, since $c/a \approx 2$.
[e] The term "fast" refers to a temperature where the high-temperature phase β-Ga_2Se_3 is stable.

2. If a *redox reaction* is energetically favoured, it will follow as a second step, even if the ion diffusion into the volumes of the crystals is impossible due to a densely packed structure. The redox reaction first requires electron exchange, ion transport comes thereafter. As a consequence, the reduced and oxidised atoms will have to change their bonds and coordination polyhedra by slight displacements (example: reaction A). Since the oxidation states of all atoms now are equal to those in the product of the reaction, the coordination polyhedra

should look similarly to those in the product. If this step results in the formation of channels or break up of rigid layers this will be helpful for subsequent ion exchange between the two crystals.

3. From this point onwards the *ion diffusion* can start unhindered throughout both crystals. This is much easier if at least one structure is ion conductive as in reaction B. As soon as ion diffusion has begun it may block its own transportation paths. Thus, this process becomes difficult for large volumes. The ion exchange between the two crystals is finally limited by diffusion, which is only driven by maximising the entropy of the system, as expected for reaction E.

We like to add that steps 1–3 help to evade the barrier of activation energy, so that high temperatures or even melting of the two compounds can be avoided. In the case of the investigated formation of $Cu(In,Ga)Se_2$ the quaternary chalcopyrite compound is produced on glass substrate below 570 °C whereas single crystal growth from the melt requires working above the melting point of 812 °C [29].

4.9. The influence of sodium doping on the reactions

If Na^+ is present either by adding a sodium dopant or by diffusion out of the soda lime glass substrate, it will presumably occupy the same site as Cu^+ due to its univalent oxidation state. This, however, leads to Na^+ point defects which we assume to be much less mobile than Cu^+ cations, since the cation radius of Na^+ is 1.5 times as large as that of Cu^+ and, more important, the Na–Se bond is more stable than the Cu–Se bond. The latter is expressed by the difference of the electronegativities of the concerning elements (EN(Na) = 0.9, EN(Cu) = 1.9, EN(Se) = 1.6 [76]) calculated from the binding enthalpies. Comparing the heat of formation of sodium selenides to isostructural copper selenides, e.g., $\Delta H(Na_2Se) = -343\,kJ/mol$ [77] and $\Delta H(Cu_2Se) = -59\,kJ/mol$ [78] justifies supports this assumption. The latter comparison is admissible, since the crystal structure of Na_2Se [79] belongs to the CaF_2 structure type, which is a supergroup of the β-Cu_2Se crystal structure. Replacing a Cu^+ cation in the β-Cu_2Se structure by Na^+ will introduce a distortion of the tetrahedral neighbourhood of the Cu^+ cations due to the tighter bonded $[NaSe_4]^{7-}$ tetrahedra. Thus, we expect the diffusion rate to decrease, if Na^+ cations are incorporated into the selenide structures. In α-$CuInSe_2$ the Na^+ concentration within the bulk is limited typically to 1 at‰ and additional Na^+ cations will accumulate at the surface [80]. Can this low Na^+ bulk concentration (assumed to be similar in all regarded reactants) really lower the speed of the solid-state reactions in Table 8, which all require the exchange of cations between the involved starting compounds?—A Na^+ concentration of 1 at‰ within the chalcopyrite structure corresponds to one Na^+ cation among $5 \times 5 \times 2\frac{1}{2}$ unit cells of $CuInSe_2$, or a cube of $(2.9\,nm)^3$. Let us assume the volume in which cation diffusion is inhibited by one Na^+ cation to be $1\,nm^3$ (this corresponds to the distance of the fifth(!) nearest neighbour) a volume fraction of just 41‰ is affected. Therefore, the effect of Na^+ cations on the grain surfaces, where crystal growth occurs, has to be taken into account and, moreover, seems to be much more important. Rudmann [81] proposes a model, in which Na^+ cations act as surfactant, passivating the surfaces of the grain boundaries. Indeed, a delayed $CuInSe_2$ formation was observed while annealing SEL with a constant heating rate and NaF having been added to the precursor [82]. For substrate temperatures lower than 500 °C during PVD, Rudmann et al. [83] showed that Na^+ impedes the intermixing of Cu^+, Ga^{3+} and In^{3+} cations in the quaternary chacopyrite. Similarly, the intermixing of a bilayer of α-$CuInSe_2$ and α-$CuGaSe_2$ prepared during PVD is lowest, if sodium doping is applied [71]. All these observations correspond to our observation, that the interdiffusion reaction of α-$CuInSe_2$ with α-$CuGaSe_2$ (reaction E) remains incomplete [5] for sodium-doped precursors when tempering SEL. This seems to contradict SEM pictures (Fig. 17a,b) taken after the annealing, which unambiguously show larger grains with sodium doping than without, as frequently reported [84]. Powder X-ray diffraction on these samples shows that phase separation has occurred induced by sodium doping. A well crystallised fraction of α-$CuInSe_2$ coexists besides fine-grained α-$Cu(In,Ga)Se_2$ with varying gallium content (Fig. 17d). This is explained easily by taking the different formation reactions of these compounds into account. In the SEL process $CuInSe_2$ is formed by the redox reaction A or B, whereas $Cu(In,Ga)Se_2$ forms via the pure diffusion reactions D and E. The influence of sodium doping on each single reaction must be taken into account separately. We first discuss the annealing of a SEL precursor.

In the chalcopyrite synthesis by annealing SEL sodium doping is required for the capture of gaseous selenium during the process by a sodium polyselenide surface layer [86] thermodynamically proven [6]. Moreover, the dopant acts as an internal catalyst acting dependent on the selenium concentration. For massive selenium excess it impedes reaction A due to formation of $CuSe_2$ below 332 °C [5]. If the temperature is raised above 377 °C reaction B will proceed quickly. When selenising SEL in slight excess reaction B is to replace reaction A at temperatures lower than 377 °C [4]. In both cases reaction B is promoted facilitating the growth of large α-$CuInSe_2$ crystallites (cf. Section 4.2). The expected decreased cation diffusion rate is not critical for the redox reactions A or B due to the short diffusion paths in InSe. The reduced cation diffusivity becomes crucial for reaction E neither involving electron transfer nor β-Cu_2Se as cation conductive reactant. Thus, the reaction time exceeds the value estimated in Section 4.5.

In the PVD process the important formation reactions are Cγ and D with the common reaction equation β-$Cu_2Se + (In,Ga)_2Se_3 \rightarrow \alpha$-$Cu(In,Ga)Se_2$. As no redox

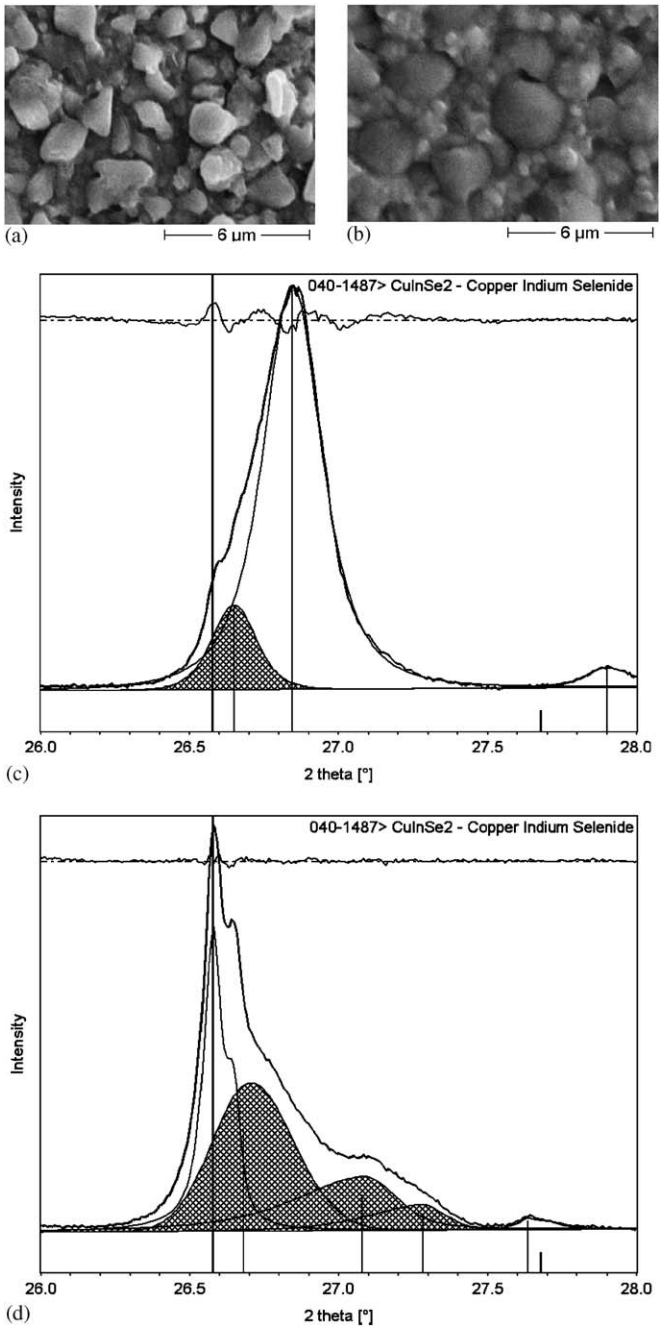

Fig. 17. The absorber material after annealing SEL up to 425 °C [5]. SEM pictures of the processed absorbers, a) without and with sodium dopant (b). The corresponding powder diffractograms (Cu-$K\alpha$ radiation) of the 112 reflection were used to estimated the crystal size by the Scherrer formula [85]. (c) Without doping: The main peak refers to $CuIn_{0.75}Ga_{0.25}Se_2$ (crystal size: 39 nm) besides residual InSe (58 nm) visible under the left shoulder. (d) With sodium dopant added we observe a phase separation into well-crystalline $CuInSe_2$ (>100 nm) and $CuIn_{1-x}Ga_xSe_2$ ($0 \leqslant x \leqslant 0.60$) with a crystal size of about 27 nm (fitted by the three shaded peaks). The sodium dopant shows two effects: First, it promotes reaction B resulting in large grains of $CuInSe_2$, second it impedes the interdiffusion reaction D observed as phase separation.

mechanism is involved to break up bonds the reaction speed is expected to decrease due to sodium doping. Indeed, a decrease of the grain size and the formation of defects caused by sodium doping has been found [66]. Therefore, the sodium doping has been recommended at the end of the chalcopyrite formation process after the growth of large $Cu(In,Ga)Se_2$ grains has finished enabling to profit from electrical enhancements [83]. Na^+ cations are unlikely to diffuse into the $CuIn(Ga)Se_2$ grains but can still terminate dangling selenium bonds on their surfaces. This mechanism is already well-known for saturating dangling silicon bonds [70] by hydrogenation of silicon technically applied for the production of amorphous silicon solar cells. Moreover, it has been calculated that the recombination of charge carriers at the grain boundaries is impeded, if Na^+ replaces Cu^+ cations on the {112} surfaces of α-$CuInSe_2$ grains [3].

4.10. Recommended reactions resulting in large grains with fewer defects

The formation of large grains of α-$CuIn(Ga)Se_2$ is promoted by reaction mechanisms allowing easy cation exchange. Since the production of α-$CuIn(Ga)Se_2$ thin films is currently done by different methods, we will discuss the three main ways of production separately.

4.10.1. Synthesis by annealing SEL

This method starts from the elements, forming binary selenide compounds serving as reactants for the reactions described above. The first compound will always be In_4Se_3 [6] together with a copper selenide depending on the amount of selenium and the usage of a sodium dopant. By setting the conditions such that In_4Se_3 and $CuSe_2$ will form as first compounds, the chalcopyrite $CuInSe_2$ cannot form, as discussed in Section 4.6.1. Above the thermal decomposition of $CuSe_2$ taking place at 332 °C [19] elemental selenium will be released according to

$$CuSe_2 \rightarrow \gamma\text{-}CuSe + Se$$

which is taken up by In_4Se_3 and further selenised to InSe. Above this temperature reaction A can start, however its reaction speed is quite low. By increasing the temperature rapidly further above 377 °C, γ-CuSe decomposes into β-Cu_2Se and selenium [19], so that reaction B can start. Due to the fact that at this point almost the complete amount of copper present in the precursor has been transformed into β-Cu_2Se crystals, the compound α-$CuInSe_2$ can quickly form and develop large grains, since this reaction is supported by the cation conductivity of β-Cu_2Se. Therefore, a beneficial temper process of SEL should allow the metallic precursor to completely selenise in selenium excess conditions before initiating reaction B by thermal decomposition of γ-CuSe.

The reaction path of gallium was shown to be separate from those of indium not starting below 400 °C [5]. Consequently, the interdiffusion of the two chalcopyrite crystal structures (reaction E) cannot start before that. This final step remains incomplete in the case of sodium doping as described in Section 4.9.

Single phase α-$CuIn_{0.75}Ga_{0.25}Se_2$ can be obtained by selenising a metallic alloy, first at poor selenium supply at 400 °C, followed by a second selenisation step in excess conditions at 500 °C [42]. Reaction B cannot proceed until additional selenium is offered whereas reaction D requires just a minimum temperature of 425 °C. If, consequently, the selenium supply starts at 425 °C, reactions B and D will coincide in time initiating reaction E. By this way single phase Cu(In,Ga)Se_2 can be obtained despite sodium doping without extensive annealing.

4.10.2. Synthesis by PVD

As discussed in Section 4.3 the formation of α-$CuInSe_2$ can be achieved by reaction of β-Cu_2Se with either the β- or the γ-phase of In_2Se_3. Comparing both the reactions Cβ and Cγ, we estimate the first reaction to be superior compared to reaction Cγ due to the β-In_2Se_3 phase being a layered structure which can easier facilitate cation exchange than γ-In_2Se_3. Thus reaction Cβ should result in larger grains and fewer defects than Cγ at identical reaction conditions like temperature and time. We further expect reaction Cβ to be especially advantageous in PVD processes, in which an β-In_2Se_3 layer is deposited during the first stage (by adjusting a slight indium excess) and copper and selenium is offered in a second stage. Then, the offered Cu^+ cations can diffuse into between the motifs of β-In_2Se_3.

However, since {110}/{102} platelets of α-$CuInSe_2$ contain fewer defects than {112} facets do [66], one should prefer reaction Cγ despite its missing possibility of cation transport as it is offered in the layered structure of β-In_2Se_3.

5. Conclusion

We have analysed the crystal structures taking part in the formation of Cu(In,Ga)Se_2 with respect to their epitaxial relations. For indium and copper selenides many possibilities for epitaxy exist, which is caused by the similar cation radii in these compounds. All solid-state reactions that we have experimentally verified previously, could be shown to be epitaxially promoted. Furthermore, we have derived one additionally possible reaction path, called Cβ, which could be observed recently. Despite our extensive and careful search for epitaxially promoted solid-state reactions, there might exist additional reaction paths, which we have overlooked.

For reactions A–D we have identified epitaxial relations, for reaction E we even find topotaxy of the reactants. Each reaction was individually described and conclusions concerning the reaction rate were drawn. The most important mechanisms to promote solid-state reactions in low temperature thin film crystallisation of Cu(In,Ga)Se_2 identified, are epitaxy, topotaxy, redox reactions breaking up bonds and ion conductive starting compounds. We have derived the formation reactions of ternary compounds starting from solid-state binary selenides. The enthalpies of formation to form the ternary compounds from the binaries are small (Table 1) compared to the formation of the binary compounds from the elements [6]. We believe this to be the essential criterion, if our crystallographic model succeeds to predict solid-state reactions by simply comparing the crystal structures of the educts. We like to emphasise that other solid-state reactions not exploiting epitaxy are not forbidden, however, the reaction speed of epitaxial-assisted reaction mechanisms is higher making the latter reactions dominating. In this spirit studying the crystal structures of all possible reactant phases for a solid-state product is a worthwhile task to recognise and adjust the optimal experimental prerequisites to attain solid-state crystal growth at low temperatures.

Acknowledgments

The authors are especially grateful to Helmuth Zimmermann (Univ. Erlangen) for his continuous assistance in matters of space group symmetry. For discussing the effect of sodium the first author thanks Dominik Rudmann (Flisom AG, Zurich) and, for his assistance in search of literature about epitaxy, Theo Hahn (RWTH Aachen). Moreover, we acknowledge funding of Bayerische Forschungsstiftung and Bundesministerium für Umwelt, Naturschutz und Reaktorsicherheit—Fachbereich Erneuerbare Energien.

References

[1] U. Rau, H.W. Schock, Appl Phys A—Mater 69 (1999) 131–147.
[2] F. Karg, Proc. of the 23rd IEEE Photovoltaic Specialists Conference, Louisville, 1993, pp. 441–446.
[3] C. Persson, A. Zunger, Phys. Rev. Lett. 91 (26) (2003) 266401.
[4] A. Brummer, V. Honkimäki, P. Berwian, V. Probst, J. Palm, R. Hock, Thin Solid Films 437 (1–2) (2003) 297–307.
[5] F. Hergert, R. Hock, A. Weber, M. Purwins, J. Palm, V. Probst, J. Phys. Chem. Solids 66 (11) (2005) 1903–1907.
[6] F. Hergert, S. Jost, R. Hock, M. Purwins, J. Palm, Thin Solid Films, 2006, in press.
[7] M.A. Contreras, B. Egaas, P. Dippo, J. Webb, J. Granata, K. Ramanathan, S. Asher, A. Swartzlander, R. Noufi, Proc. 26th IEEE Photov. Spec. Conf., IEEE, New York, 1997 (p. 359).
[8] A.M. Gabor, J.R. Tuttle, D.S. Albin, M.A. Contreras, R. Noufi, A.M. Hermann, Appl. Phys. Lett. 65 (2) (1994) 198–200.
[9] M.A. Contreras, B. Egaas, D. King, A. Swartzlander, T. Dullweber, Thin Solid Films 361–362 (2000) 167–171.
[10] D. Lincot, J.F. Guillemolles, S. Taunier, D. Guimard, J. Sicx-Kurdi, A. Chaumont, O. Roussel, O. Ramdani, C. Hubert, J.P. Fauvarque, N. Boderau, L. Parissi, P. Panheleux, P. Fanouillere, N. Naghavi, P.P. Grand, M. Benfarah, P. Mogensen, O. Kerrec, Sol. Energy 77 (6) (2004) 725–737.
[11] A. Bravais, J. Ec. Polytech. 20 (1851) 101–276.
[12] P. Niggli, Z. Kristallogr. 58 (1923) 490–521.
[13] J.D.H. Donnay, D. Harker, Am. Mineral. 22 (1937) 446–467.
[14] P. Hartman, Can. Mineral. 16 (1978) 387–391.
[15] R.F.P. Grimbergen, H. Meekes, P. Bennema, C.S. Strom, L.J.P. Vogels, Acta Crystallogr. A 54 (1998) 491–500.
[16] T. Hahn, International Tables for Crystallography, Vol. A, Space-Group Symmetry, Reidel, Dordrecht/Boston, 1983.
[17] W. Kraus, G. Nolze, Federal Institute for Materials Research and Testing, Berlin, PowderCell for Windows, Vers. 2.3, 1999.

[18] R.D. Shannon, Acta Crystallogr. A 32 (1976) 751–767.
[19] T.B. Massalski, Binary Alloy Phase Diagrams, American Society for Metals, Metals Park, Ohio, 1986.
[20] R.D. Heyding, Can. J. Chemistry 55 (10) (1966) 1233–1236.
[21] W. Borchert, Z. Kristallogr. 106 (1945) 5–24.
[22] Z. Vucic, J. Gladic, Fizika A (Zagreb) 9 (1) (2000) 9–26.
[23] V.A. Chatov, T.P. Iorga, P.N. Inglizjan, Fizika i Tekhnika Poluprovodnikov [Sov. Phys. Semicond + .] 14 (4) (1980) 807–809.
[24] K. Yamamoto, S. Kashida, Solid State Ionics 48 (1991) 241–248.
[25] T. Kanashiro, Y. Kishimoto, T. Ohno, Y. Michihiro, Solid State Ionics 40/41 (1) (1990) 308–311.
[26] H. Hahn, W. Klingler, Z. Anorg. Chem. 259 (1949) 135–142.
[27] G. Ghemard, S. Jaulmes, J. Etienne, J. Flahaut, Acta Crystallogr. C 39 (1983) 968–971.
[28] L. Pauling, L.O. Brockway, Z. Krist. 82 (1932) 188–194.
[29] T. Gödecke, T. Haalboom, F. Ernst, Z. Metallkd. 91 (8) (2000) 622–662.
[30] H. Matsushita, A. Katsui, T. Takizawa, J. Cryst. Growth 237–239 (2002) 1986–1992.
[31] W. Paszkowicz, R. Lewandowska, R. Bacewicz, J. Alloy Compd. 362 (2004) 241–247.
[32] L. Mandel, R.D. Tomlinson, M.J. Hampshire, J. Appl. Crystallogr. 10 (1977) 130–131.
[33] D.K. Suri, K.C. Nagpal, G.K. Chadah, J. Appl. Crystallogr. 22 (6) (1989) 578–583.
[34] J.-B. Li, M.-C. Record, J.-C. Tedenac, Z. Metallkd. 94 (4) (2003/04) 381–389.
[35] A. Pfitzner, H.D. Lutz, J. Solid State Chem. 124 (1996) 305–308.
[36] W. Klemm, H. Vogel, Z. Anorg. Allg. Chem. 219 (1) (1934) 45–64.
[37] S.A. Semiletov, Kristallografiya USSR 3 (1958) 288–292; S.A. Semiletov, Soviet Physics—Crystallography 3 (1958) 292–297.
[38] J. Rigoult, A. Rimsky, A. Kuhn, Acta Crystallogr. B 36 (1980) 916–918.
[39] F. Jellinek, H. Hahn, Z. Naturforsch. 16B (1961) 713–715.
[40] K. Cenzual, L.M. Gelato, M. Penzo, E. Parthe, Acta Crystallogr. B 47 (4) (1991) 433–439.
[41] G. Jander, E. Blasius: Lehrbuch der analytischen und präparativen anorganischen Chemie,, 12th ed, Hirzel, Stuttgart, 1983 (p. 106).
[42] V. Alberts, Semicond. Sci. Tech. 19 (2004) 65–69.
[43] R. Walther, H.J. Deiseroth, Z. Kristallogr. 210 (1995) 359.
[44] K. Osamura, Y. Murakami, Y. Tomiie, J. Phys. Soc. Jpn. 21 (1966) 1848.
[45] V. Milman, Acta Crystallogr. B 58 (2002) 423–436.
[46] J.C.W. Folmer, F. Jellinek, J. Less-Common Met. 76 (1–2) (1980) 153–162.
[47] S. Stolen, H. Fjellvag, F. Gronvold, J. Sipowska, E.F. Westrum Jr, J. Chem. Thermodyn. 28 (7) (1996) 753–766.
[48] U. Schwarz, H. Hillebrecht, Z. Kristallogr. 210 (1995) 342–347.
[49] G. Gattow, Z. Anorg. Chem. 340 (5–6) (1965) 312–318.
[50] Gmelin Handbuch der Anorganischen Chemie, eigth ed. System-Nr. 10: Selenium, Suppl. Vol. A2, Springer, Berlin, 1980, pp. 86–101.
[51] P. Cherin, P. Unger, Inorganic Chemistry (Washington D.C) 6 (1967) 1589–1591.
[52] Ref. [50], 241–244.
[53] H. Krebs, Z. Anorg. Allg. Chem. 265 (1951) 156–168.
[54] L. Royer, Bull. Soc. Franc. Mineral. Cristallogr. 51 (1928) 7–159.
[55] T. Wada, N. Kohara, T. Negami, M. Nishitani, J. Mater. Res. 12 (6) (1997) 1456–1462.
[56] L. Vegard, H. Schjelderup, Phys. Zeitschrift 18 (1917) 93–96.
[57] L. Vegard, Z. Phys. 5 (1921) 17–26.
[58] A. Koma, K. Yoshimura, Surf. Sci. 174 (1986) 556–560.
[59] S. Kim, W.K. Kim, R.M. Kaczynski, R.D. Acher, S. Yoon, T.J. Anderson, O.D. Crisalle, E.A. Payzant, S.S. Li, J. Vac. Sci. Technol. A 23 (2) (2005) 310–315.
[60] M. Purwins, A. Weber, P. Berwian, G. Müller, F. Hergert, S. Jost, R. Hock, J. Cryst. Growth, 2006, accepted.
[61] J.S. Park, Z. Dong, S. Kim, J.H. Perepezko, J. Appl. Phys. 87 (8) (2000) 3683–3690.
[62] S. Verma, N. Orbey, R.W. Birkmire, T.W.F. Russel, Prog. Photovoltaics 4 (5) (1996) 341–353.
[63] N. Orbey, H. Hichri, R.W. Birkmire, T.W.F. Russel, Prog. Photovoltaics 5 (4) (1997) 237–247.
[64] N. Orbey, G. Norsworthy, R.W. Birkmire, T.W.F. Russel, Prog. Photovoltaics 6 (2) (1998) 79–86.
[65] F.O. Adurodija, M.J. Carter, R. Hill, Sol. Energy Mat. Sol. C. 37 (1995) 203–216.
[66] N. Ott, G. Hanna, U. Rau, J.H. Werner, H.P. Strunk, J. Phys.-Condens. Mat. 16 (2004) S85–S89.
[67] S. Chaisitsak, A. Yamada, M. Konagai, Jpn. J. Appl. Phys. 41 (2002) 507–513.
[68] C. Amory, J.C. Bernede, E. Halgand, S. Marsillac, Thin Solid Films 431–432 (2003) 22–25.
[69] S. Nishiwaki, S. Siebentritt, M. Giersig, M.C. Lux-Steiner, J. Appl. Phys. 94 (10) (2003) 6864–6870.
[70] R.A. Street, Hydrogenated Amorphous Silicon, Cambridge University Press, Cambridge, 1991.
[71] O. Lundberg, J. Lu, A. Rockett, M. Edoff, L. Stolt, J. Phys. Chem. Solids 64 (2003) 1499–1504.
[72] D.J. Schroeder, G.D. Berry, A.A. Rockett, Appl. Phys. Lett. 69 (26) (1996) 4068–4070.
[73] W.K. Kim, S. Kim, E.A. Payzant, S.A. Speakman, S. Yoon, R.M. Kaczynski, R.D. Acher, T.J. Anderson, O.D. Crisalle, S.S. Li, V. Craciun, J. Phys. Chem. Solids 66 (11) (2005) 1915–1919.
[74] H.R. Thirsk, E.J. Whitmore, Trans. Farad. Soc. 36 (1940) 565–574.
[75] A. Neuhaus, Fortschr. d. Mineral. 29/30 (1950/1951) 136–296.
[76] L. Pauling, The Nature of the Chemical Bond and The Structure of Molecules and Crystals, third ed, Cornell University Press, Ithaca, NY, 1960.
[77] E.A. Maiorova, A.G. Morachevskii, Zhurnal Prikladnoi Khimii (Sankt–Peterburg, Russia) 53 (2) (1980) 276–279.
[78] K. Mills, Thermodynamic Data for Inorganic Sulphides. Selenides andn Tellurides, Butterworths, London, 1974.
[79] E. Zintl, A. Harder, B. Dauth, Z. Eletrochem. 40 (1934) 588–593.
[80] D.W. Niles, K. Ramanathan, F. Hasoon, R. Noufi, B.J. Tielsch, J.E. Fulghum, J. Vac. Sci. Technol. A 15 (1997) 3044–3049.
[81] D. Rudmann, Effects of sodium on growth and properties of Cu(In,Ga)Se_2 thin films and solar cells, Thesis, ETH Zurich, 2004, pp. 140–152.
[82] D. Wolf, G. Müller, W. Stetter, F. Karg, in: J. Schmid, H.A. Ossenbrink, P. Helm, H. Ehmann, E.D. Dunlop (Eds.), Proceedings of the 2nd World Conference on Photovoltaic Solar Energy Conversion, Vienna, Vol. 2. 1998, p. 2426.
[83] D. Rudmann, D. Bremaud, A.F. da Cunha, G. Bilger, A. Strohm, M. Kaelin, H. Zogg, A.N. Tiwari, Thin Solid Films 480–481 (2005) 55–60.
[84] V. Probst, J. Rimmasch, W. Stetter, H. Harms, W. Riedl. J. Holz, F. Karg, Proc. 13th EC PVSEC, Nice, 1995, pp. 2126–2132.
[85] R.W. James, The Optical Principles of the Diffraction of X-rays—Vol. II: The Crystalline State, Bell & Sons, London, 1948 (pp. 513–589, Chapter X).
[86] D. Braunger, D. Hariskos, G. Bilger, U. Rau, H.W. Schock, Thin Solid Films 361–362 (2000) 161–166.